Nuclear masses in the fermion dynamical symmetry model

Xiao-Ling Han*
Department of Physics and Astronomy, University of Tennessee, Knoxville, Tennessee 37996
and Department of Physics, Jilin University, Changchun, Jilin, China

Cheng-Li Wu*
Department of Physics and Atmospheric Science, Drexel University, Philadelphia, Pennsylvania 19104;
Department of Physics and Astronomy, University of Tennessee, Knoxville, Tennessee 37996;
Joint Institute for Heavy-Ion Research, Oak Ridge, Tennessee 37831;
and Department of Physics, Jilin University, Changchun, Jilin, China

Da Hsuan Feng†
Department of Physics and Atmospheric Science, Drexel University, Philadelphia, Pennsylvania 19104

Mike W. Guidry‡
Department of Physics and Astronomy, University of Tennessee, Knoxville, Tennessee 37996
and Physics Division, Oak Ridge National Laboratory, Oak Ridge, Tennessee 37831
(Received 28 May 1991)

A new microscopic nuclear mass formula is derived from the fermion dynamical symmetry model. A Strutinsky-like spherical single-particle shell correction is introduced, but the principle part of the pairing and deformation are treated microscopically through the pairing and quadrupole-quadrupole two-body interaction, without introducing a deformed mean-field or BCS approximation. The results are in excellent agreement with existing mass data in the actinide region and suggest the possibility of a new region of superheavy elements near $Z=114$ and $N=164$. This mass formula has been utilized in the study of r processes in astrophysical problems with encouraging preliminary results.

PACS number(s): 21.60.Ev, 21.60.Fw, 21.10.Dr

I. INTRODUCTION

The masses of nuclei contain fundamental information about the physical Universe. Indeed, one of the aims in theoretical nuclear physics is to provide a sufficiently accurate mass formula in the β-stable regions so that extrapolation into unknown neutron- and proton-rich regions can be carried out with a reasonable degree of confidence. Such extrapolations have important consequences in other fields of physics as well. An archetypical application of using the masses of such exotic yet unknown nuclei is in astrophysics studies [1], where the heavy nuclear masses are important ingredients in the r-processes and galactic age determinations [2].

There exist many versions of mass formulas [3], and the number of parameters in these formulas range from as few as 12 to as many as 928. Roughly speaking, they can be grouped into three classes: (I) formulas that are interpolated and extrapolated from known nuclear systematics, (II) formulas that are based on phenomenological nuclear models, and (III) formulas that are based on microscopic nuclear models. If the physics dictates that one needs to go only slightly beyond the known regions, then some of the phenomenological formulas in classes I and II may be accurate and convenient to use. However, if the physics requires knowledge of nuclear masses far from β stability, as in the astrophysical processes, the microscopic formulas from III would seem to be preferred, because the more physics one incorporates in the formula the more reliable we may hope it to be for distant extrapolation (unless new physics of a radically different nature appears in the unknown region of interest). The traditional microscopic mass formulas are based on the deformed shell model plus a Strutinsky shell correction [4]; the Möller-Nix formula is a typical example [5].

In the past few years, a new microscopic fermion dynamical symmetry model (FDSM) for nuclear structure has been developed [6]. This model is based on an effective interaction theory of the spherical shell model and is motivated by the concept of dynamical symmetry as a truncation principle. One of the first tests of the FDSM was to ascertain whether it can describe nuclear masses in the actinide region ($Z>82$, $N>126$). Simplicity in the symmetry was the reason for choosing the actinide region: According to the model, the shell structure here possesses a rather simple dynamical symmetry structure [$Sp^{\pi}(6)\times Sp^{\nu}(6)$ for the nucleons in the normal parity levels and $Su^{\pi}(2)\times Su^{\nu}(2)$ in the abnormal parity levels]. In the first version of the FDSM mass formula (we shall refer to it as version I) [7], not only were we able to obtain excellent results in fitting the 332 known nuclear masses in the actinide region (the root-mean-square devi-

*Electronic address: cwu@utkvx.bitnet.
†Electronic address: feng@duvm.bitnet.
‡Electronic address: guidry@utkvx.bitnet.

ation, rms, was 0.34 MeV, which is better than that of the Möller-Nix mass formula in this region), but we found the first evidence for the dynamical Pauli effect, which turns out to be of central importance in understanding the saturation of deformation for normally deformed nuclei [8], the formation of superdeformed nuclei [9], and a variety of other phenomena [10]. Still, several important questions regarding this mass formula persist. Attempts to answer these questions have led to an in-depth reformulation of the mass formula (the new formula will be termed version II). The purpose of this paper is to describe version II.

Version II is based on three principle ingredients: (1) the dynamical symmetry limits of the FDSM, (2) the inclusion of diagonal matrix elements of symmetry-breaking interactions, and (3) a Strutinsky-like spherical single-particle (s.p.) and pairing shell correction. The result is that version II is able to produce an excellent fit of the 332 known nuclei with a better rms error of 0.22 MeV (vs the 0.34 MeV of version I), and parameters that are fewer in number and have a clearer microscopic interpretation. More important, the new approach is rather simple and can straightforwardly be extended to other mass regions. In Sec. II, we shall give an outline of the difficulties encountered by version I. In Sec. III, a Strutinksy-like approach for the spherical s.p. shell correction and a pairing shell correction are discussed in detail. These corrections are of great conceptual and practical importance in deriving version II of our mass formula. This is followed in Sec. IV by a comprehensive discussion of the present formulation. Finally, in Sec. V the results and conclusions are presented.

II. A BRIEF OUTLINE OF VERSION I OF THE FDSM MASS FORMULA

We have previously obtained a microscopic formula for heavy and superheavy nuclei ($82 \le Z \le 126$ and $126 \le N \le 184$, version I) [7] that can be written as follows:

$$M(Z,N) = M(^{208}\mathrm{Pb}) + n_p M_p + n_n M_n + \langle \mathbf{H}_{\mathrm{FDSM}} \rangle \ . \quad (2.1)$$

In Eq. (2.1), $M(^{208}\mathrm{Pb})$ is the closed-shell lead mass (assumed known), $\langle \mathbf{H}_{\mathrm{FDSM}} \rangle$ is the FDSM Hamiltonian expectation value, $n_p = Z - 82$ and $n_n = N - 126$ are the valence proton and neutron numbers, respectively, and M_p and M_n are the free proton and neutron masses, respectively. Although the agreement obtained from this mass formula is rather impressive (a 16-parameter fit to 332 known nuclei in the actinide region yields a rms error of 0.34 MeV), it is designed only for heavy and superheavy nuclei. Hence one is immediately faced with a problem of how to extend it to other regions of the periodic table.

It is well known that an accurate treatment of the single-particle energies in any microscopic formulation of masses is difficult. For example, it is for this reason that one does not expect the shell model to produce sufficiently accurate masses for medium-heavy and heavy nuclei. Not only is the shell model faced with the inherent difficulty of diagonalizing an astronomically large many-body Hamiltonian matrix, but the s.p. energies are not sufficiently accurate to allow one to extract information confidently about the masses. For example, a mere 0.1 MeV uncertainty in the s.p. energies could result in errors as large as several MeV in a mass calculation for a nucleus with 10^2 particles.

In traditional mass calculations the large dimension problem is overcome by utilizing the deformed mean-field approximation, while the difficulty of the accuracy of s.p. energies is treated by the Strutinsky procedure [4]. The Strutinsky procedure provides a clever empirical recipe to compute shell corrections to the smooth liquid drop mass from a given set of deformed s.p. energies, and the nuclear mass is then obtained by combining the liquid drop mass and the shell corrections.

On the other hand, the FDSM elegantly solves the many-body shell-model problem without the deformed mean-field approximation. This means that important many-body correlations may be treated more accurately, but the problem associated with a lack of precise knowledge of the s.p. energies is even more serious here since in the FDSM symmetry limits one assumes that the spherical s.p. energies are degenerate. This difficulty must be overcome before the FDSM can be utilized as a general theoretical framework to compute nuclear masses.

An important question one may ask at this point is why version I, which lacks the proper spherical s.p. splittings, should work so well. The reason turns out to be rather simple. The expectation value of the FDSM Hamiltonian $\langle \mathbf{H}_{\mathrm{FDSM}} \rangle$ is essentially a quadratic function of n_p and n_n, plus some symmetry correction terms. The latter are not smooth functions of n_p and n_n, and correspond physically to nuclear shape changes. For example, the transition from Su_2 to Su_3 signals a spherical to deformed shape transition, while that of Su_3 symmetric $(\lambda,0)$ to nonsymmetric $(\lambda,\mu \neq 0)$ representations corresponds to an axial to triaxial deformed shape transition [10(b),10(c)]. It is likely that these symmetry correction terms are the primary source for the parts of the usual Strutinsky shell correction that are not smooth. These parts, which are mostly associated with deformation and pairing effects, are treated microscopically in the FDSM at the two-body level without deformed mean-field and BCS-type approximations. What remains (which seemingly is missing in version I) is the Strutinsky-like shell correction due to the *spherical* s.p. energy splitting and the *spherical* liquid drop mass; these are presumably smooth functions of n_p and n_n, and can be approximated by quadratic functions. Higher powers of n_p and n_n in the expansion with respect to the closed-shell $^{208}\mathrm{Pb}$ should be small in comparison to the leading-order terms since $n_p/82$ and $n_n/126$ are relatively small numbers. This means that once the coefficients of the quadratic functions of $\langle \mathbf{H}_{\mathrm{FDSM}} \rangle$ are determined empirically, both the spherical liquid drop mass and the spherical s.p. shell correction contributions are implicitly included. Thus, these important physical effects are effectively present in version I, but they may be entangled with other contribu-

tions to the coefficients of the quadratic expansion in particle numbers.

The preceding argument implies that version I cannot be easily extended to other mass regions, since higher-order terms in the expansion of the spherical liquid drop mass and the spherical s.p. shell corrections may no longer be negligible. Therefore, in order to extend the FDSM mass formula to other mass regions, and to allow an unambiguous microscopic interpretation of parameters, one is compelled to incorporate the spherical liquid drop mass and to compute *explicitly* the spherical s.p. shell correction. Since the spherical liquid drop mass formula is known [5], the key to this task is to find a way to compute the spherical s.p. shell corrections accurately and efficiently. In the next section, we shall show how this can be accomplished.

III. THE SPHERICAL SINGLE-PARTICLE AND PAIRING SHELL CORRECTIONS

First, let us consider the spherical single-particle energies for neutrons and protons:

$$E_{\rm sh}^{\rm s.p.}=\sum_{i=83}^{Z}\varepsilon_i^{\pi}n_i^{\pi}+\sum_{i=127}^{N}\varepsilon_i^{\nu}n_i^{\nu}\ . \tag{3.1}$$

Here the philosophy of Strutinsky plays a crucial role. We shall introduce a shell correction $M_{\rm sh}^{\rm s.p.}$ that can be computed by subtracting from $E_{\rm sh}^{\rm s.p.}$ a smooth component given by the standard Fermi-gas (FG) model:

$$M_{\rm sh}^{\rm s.p.}=M_{\rm sh}^{\rm s.p.}(Z)+M_{\rm sh}^{\rm s.p.}(N)=\left[\sum_{i=83}^{Z}\varepsilon_i^{\pi}n_i^{\pi}-[E_{\rm FG}(Z)-E_{\rm FG}(82)]+n_p\varepsilon_p\right]+\left[\sum_{i=127}^{N}\varepsilon_i^{\nu}n_i^{\nu}-[E_{\rm FG}(N)-E_{\rm FG}(126)]+n_n\varepsilon_n\right]\ . \tag{3.2}$$

In Eq. (3.2) $E_{\rm FG}(n)$ represents the Fermi-gas energy for n nucleons [11]:

$$E_{\rm FG}(Z)=(\tfrac{3}{5}Z^{5/3})C_p/R_p^2\ ,\qquad E_{\rm FG}(N)=(\tfrac{3}{5}N^{5/3})C_n/R_n^2 \tag{3.3a}$$

and

$$R_{n,p}=A^{1/3}\left[\frac{1\pm I}{(1-3\bar{\varepsilon})(1\pm\bar{\delta})}\right]^{1/3}, \tag{3.3b}$$

$$I=(N-Z)/A\ ;$$

$$\bar{\delta}=\frac{[I+\frac{3}{16}(c_1/Q)ZA^{-2/3}]}{[1+\frac{9}{4}(J/Q)A^{-1/3}]}\ , \tag{3.3c}$$

$$\bar{\varepsilon}=[-2a_2A^{-1/3}+L\bar{\delta}^2+c_1Z^2A^{-4/3}]/K\ .$$

The quantities ε_p and ε_n are the difference of energy zero points of the two s.p. energy level schemes; n_p and n_n are the number of valence nucleons, $n_p=Z-82$ and $n_n=N-126$. Since the spherical shell-model s.p. energy levels are chosen such that the first s.p. levels beyond ^{208}Pb for both protons and neutrons are set to be zero, it is convenient to define ε_p and ε_n as follows:

$$\varepsilon_p=(\tfrac{3}{5}83^{5/3}-\tfrac{3}{5}82^{5/3})C_p/R_p^2+e_p\ ,\qquad \varepsilon_n=(\tfrac{3}{5}127^{5/3}-\tfrac{3}{5}126^{5/3})C_n/R_n^2+e_n\ . \tag{3.3d}$$

Thus the constant e_p (e_n) determines the relative position of the proton (neutron) Fermi-gas s.p. level scheme with respect to the corresponding shell-model s.p. level scheme: If e_p and e_n are zero, the two s.p. schemes will coincide with each other at the 83th proton and 127th neutron; otherwise the Fermi-gas s.p. scheme will be

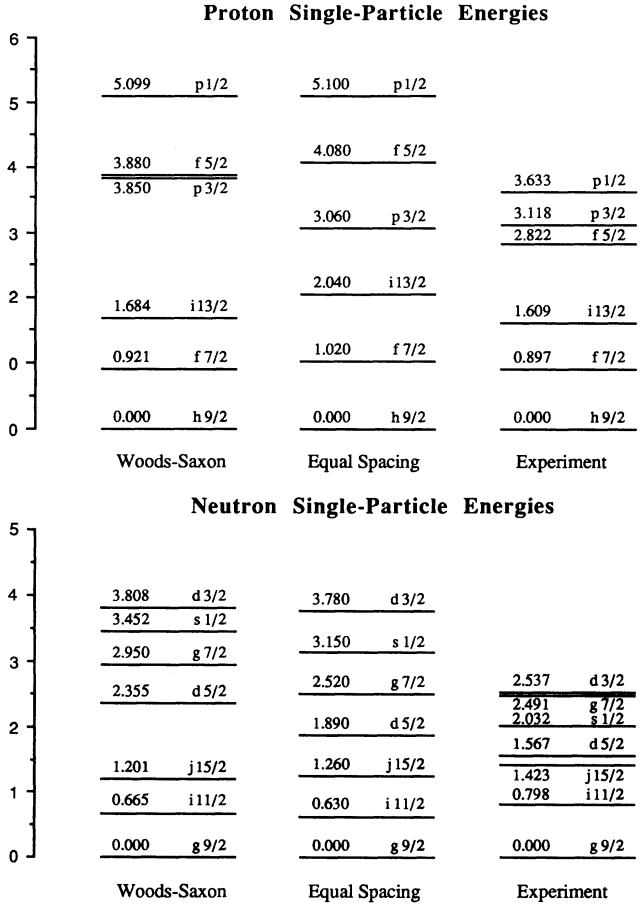

FIG. 1. Single-particle energies used in the heavy and superheavy mass calculations. The experimental single-particle energies are obtained from the spectra of ^{209}Pb and ^{209}Bi [*Table of Isotopes*, 7th ed., edited by C. M. Lederer and V. S. Shirley (Wiley, New York, 1978)].

shifted up or down with respect to the shell-model s.p. scheme. The values of e_p and e_n are determined by requiring the maximum cancellation in Eq. (3.2), or equivalently by minimizing $\sum_{Z=83}^{126} M_{\rm sh}^{\rm s.p.}(Z)^2$ and $\sum_{N=127}^{184} M_{\rm sh}^{\rm s.p.}(N)^2$. In the context of this variational principle, there are no freely adjustable parameters in the spherical s.p. shell correction $M_{\rm sh}^{\rm s.p.}$. The values and meaning of the parameters appearing in Eqs. (3.3a)–(3.3d) are [5,12] $e_p=3.212$ MeV, proton scaling parameter; $J=38.2$ MeV, symmetry energy; $e_n=3.477$ MeV, neutron scaling parameter; $L=100$ MeV, density-symmetry coefficient; $c_1=0.7403$ MeV, Coulomb energy ($\frac{3}{5}e^2/r_0$); $K=300$ MeV, compressibility coefficient; $a_2=20.85$ MeV, surface energy; $C_p=72$ MeV, neutron Fermi energy; $Q=17.7$ MeV, effective-surface stiffness; $C_n=71$ MeV, proton Fermi energy.

In the symmetry limit the FDSM pairing energies for protons and neutrons correspond to the pairing energies in a degenerate spherical s.p. scheme. Hence, the spherical s.p. energy splitting requires one to introduce a pairing shell correction term $V_{\rm sh}^{\rm pair}$ as well:

$$V_{\rm sh}^{\rm pair}=[V_\pi^{\rm pair}({\rm BCS})-V_\pi^{\rm pair}({\rm deg})]+[V_\nu^{\rm pair}({\rm BCS})-V_\nu^{\rm pair}({\rm deg})]\ . \tag{3.4}$$

In Eq. (3.4), $V_\sigma^{\rm pair}({\rm BCS})$ is the pairing energy computed for a given s.p. level scheme in the standard BCS method ($\sigma=\pi,\nu$), while $V_\sigma^{\rm pair}({\rm deg})$ is the BCS pairing energy for the degenerate s.p. level scheme, which is known analytically:

$$V_\sigma^{\rm pair}({\rm deg})=G_\sigma N^\sigma(\Omega^\sigma-N^\sigma+N^\sigma/\Omega^\sigma)\quad(\sigma=\pi,\nu)\ . \tag{3.5}$$

The symbol Ω^σ in Eq. (3.5) denotes the shell degeneracy. The BCS approximation is used here only to calculate the corrections due to the spherical s.p. splitting. The principle part of the pairing in the FDSM is treated below as a two-body interaction, as it should be. Therefore, the error in the total mass made by using the BCS approximation to compute the correction (3.4) should be small.

The pairing strength $G_\sigma^{\rm pair}$ in $V_\sigma^{\rm pair}({\rm BCS})$ is determined by requiring it to reproduce the experimental average

TABLE I. BCS pairing used in the pairing s.p. shell correction. The pairing operator is assumed to be of the form $G_\sigma^{\rm pair}\mathbf{S}_T^\dagger\mathcal{S}_T$, where $\mathbf{S}_T=\mathbf{S}+\mathcal{S}$, and $G_\pi^{\rm pair}=0.094$, $G_\nu^{\rm pair}=-0.052$ MeV, as explained in the text. Woods-Saxon single-particle energies were used.

n_π	$V_\pi^{pair}(BCS)$	n_π	$V_\pi^{pair}(BCS)$	n_π	$V_\pi^{pair}(BCS)$	n_π	$V_\pi^{pair}(BCS)$
1	0.0329	12	-1.3617	23	-2.3900	34	-2.0436
2	-0.6374	13	-1.0510	24	-3.0871	35	-1.8763
3	-0.4783	14	-1.7339	25	-2.5291	36	-2.3283
4	-1.0480	15	-1.2351	26	-3.0723	37	-2.0710
5	-0.7476	16	-1.7630	27	-2.4015	38	-2.4369
6	-1.2121	17	-1.0383	28	-2.8033	39	-2.0736
7	-0.7407	18	-1.4448	29	-2.0156	40	-2.3178
8	-1.0911	19	-1.2143	30	-2.2827	41	-1.8489
9	-0.3677	20	-2.3015	31	-1.3708	42	-1.9758
10	-0.5781	21	-1.9626	32	-1.5054	43	-1.9617
11	-0.4507	22	-2.8372	33	-1.4658	44	-2.0703
n_ν	$V_\nu^{pair}(BCS)$	n_ν	$V_\nu^{pair}(BCS)$	n_ν	$V_\nu^{pair}(BCS)$	n_ν	$V_\nu^{pair}(BCS)$
1	0.0197	16	-1.5898	31	-1.9315	46	-1.4676
2	-0.3787	17	-1.2402	32	-2.2570	47	-1.3531
3	-0.2832	18	-1.6356	33	-1.7530	48	-1.5945
4	-0.6218	19	-1.1752	34	-1.9956	49	-1.4023
5	-0.4410	20	-1.5021	35	-1.4170	50	-1.5592
6	-0.7165	21	-0.9120	36	-1.5786	51	-1.2863
7	-0.4319	22	-1.1804	37	-0.9174	52	-1.3638
8	-0.6383	23	-0.9933	38	-0.9963	53	-1.3417
9	-0.1970	24	-1.7390	39	-0.9673	54	-1.4160
10	-0.3140	25	-1.4965	40	-1.2444	55	-1.3976
11	-0.2569	26	-2.1145	41	-1.1189	56	-1.5297
12	-0.9618	27	-1.8107	42	-1.3006	57	-1.4529
13	-0.8021	28	-2.3200	43	-1.0681	58	-1.5212
14	-1.3685	29	-1.9522	44	-1.1539		
15	-1.1168	30	-2.3657	45	-1.1234		

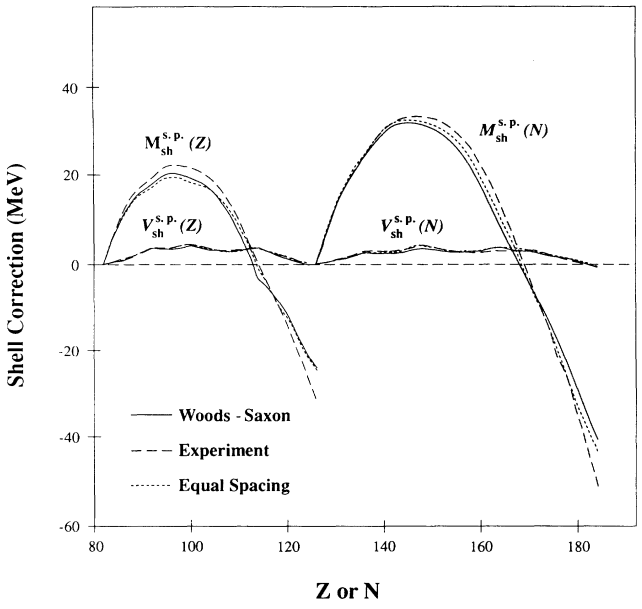

FIG. 2. The spherical s.p. shell corrections $M_{sh}^{s.p.}$ and pairing shell corrections V_{sh}^{pair} for the single-particle schemes of Fig. 1. For clarity, only results for even-even nuclei are presented.

pairing gap (even-odd mass differences) for the spherical nuclei in this region ($\Delta_n=0.86$ MeV and $\Delta_p=1.0$ MeV, see Fig. 3). However, it should be noted that the experimental even-odd mass differences do not arise from monopole pairing alone; there is a contribution from the quadrupole pairing as well. As we shall see in the next section, in order to reproduce the empirical $\Delta_n=0.86$ MeV and $\Delta_p=1.0$ MeV, the corresponding pairing gaps for an effective monopole pairing interaction are $\Delta_n=0.409$ MeV and $\Delta_p=0.605$ MeV. These are values we actually used to determine G_σ^{pair}. The strength G_σ in $V_\sigma^{pair}(\text{deg})$ is then fixed by minimizing the energy gap difference, i.e., minimizing $\sum_{Z=83}^{126}[\Delta_{BCS}(Z)-\Delta_{deg}(Z)]^2$ and $\sum_{N=127}^{184}[\Delta_{BCS}(N)-\Delta_{deg}(N)]^2$, where $\Delta_{BCS}(N)$ and $\Delta_{deg}(N)$ are the pairing gaps for $V_\sigma^{pair}(\text{BCS})$ and $V_\sigma^{pair}(\text{deg})$, respectively, and

$$\Delta_{deg}=G_\sigma\sqrt{N_\sigma(\Omega_\sigma-N_\sigma)}\quad(\sigma=\pi,\nu)\ . \tag{3.5'}$$

Therefore, just as for the spherical s.p. energy shell corrections, there are no freely adjustable parameters here. For example, if the spherical Woods-Saxon s.p. energies are used (see Fig. 1), then the values of these fixed parameters are (in MeV)

$$\begin{aligned} &G_\pi^{pair}=-0.094,\quad G_\nu^{pair}=-0.052\ ,\\ &G_\pi=-0.047,\quad G_\nu=-0.023\ , \end{aligned} \tag{3.6}$$

and the calculated BCS pairing energies $V_\sigma^{pair}(\text{BCS})$ are listed in Table I.

The behavior of the spherical s.p. shell correction $M_{sh}^{s.p.}$ and the pairing s.p. shell correction V_{sh}^{pair} for three different s.p. schemes (see Fig. 1) are shown in Fig. 2.

IV. THE FDSM STRUTINSKY MASS FORMULA

Once the spherical s.p. shell correction $M_{sh}^{s.p.}$ and pairing shell correction V_{sh}^{pair} are computed, we have version II, which we shall refer to as the *FDSM Strutinsky atomic mass formula.* It is written as follows:

$$M(Z,N)=M_{lq}^{S}+M_{sh}\ , \tag{4.1a}$$

$$M_{sh}=M_{sh}^{s.p.}+V_{sh}^{pair}+\langle \mathbf{V}_{FDSM}\rangle\ , \tag{4.1b}$$

where M_{lq}^{S} is the spherical liquid drop mass and M_{sh} is the total shell correction. We shall now discuss the various terms in detail.

(1) The spherical liquid drop mass M_{lq}^{S} is

$$\begin{aligned} M_{lq}^{S}=&M_H Z+M_n N-a_v(1-\kappa_v I^2)A+a_s(1-\kappa_s I^2)B_1 A^{2/3}+c_0 A^0\\ &+c_1\frac{Z^2}{A^{1/3}}B_3-c_4\frac{Z^{4/3}}{A^{1/3}}+f(k_f r_p)\frac{Z^2}{A}-c_a(N-Z)\\ &+W\left[|I|+\begin{cases}1/A & Z \text{ and } N \text{ odd and equal}\\ 0 & \text{otherwise}\end{cases}\right]-a_{el}Z^{2.39}-\frac{h}{A^{2/3}}\ , \end{aligned} \tag{4.2}$$

where the parameter h is nonzero only for odd-odd nuclei, and

$$B_1=1-\frac{3}{x_0^2}+(1+x_0^2)\left[2+\frac{3}{x_0}+\frac{3}{x_0^2}\right]e^{-2x_0}\ ,\quad x_0=\frac{r_0A^{1/3}}{a}\ , \tag{4.3a}$$

$$B_3=1-\frac{5}{y_0^2}\left[1-\frac{15}{8y_0^2}+\frac{21}{8y_0^3}-\frac{3}{4}\left[1+\frac{9}{2y_0}+\frac{7}{y_0^2}+\frac{7}{2y_0^3}\right]e^{-2y_0}\right]\ ,\quad y_0=\frac{r_0A^{1/3}}{a_{den}}\ , \tag{4.3b}$$

$$f(k_f r_p)=-\frac{1}{8}\frac{r_p^2e^2}{r_0^3}\left[\frac{145}{48}-\frac{327}{2800}(k_f r_p)^2+\frac{1527}{1\,209\,600}(k_f r_p)^4\right]\ . \tag{4.3c}$$

The parameters for Eqs. (4.2) and (4.3) are listed in Table II. This liquid drop mass formula is essentially taken from Ref. [5], except for the removal of the *n-n* and *p-p* pairing terms to avoid overcounting, since pairing energies have al-

TABLE II. Parameters of the spherical liquid drop model.

$M_H=7.289034$ MeV	$\kappa_v=1.911$	$c_4=c_1\frac{5}{4}\left[\frac{3}{2\pi}\right]^{2/3}$	$e^2=1.4399764$ MeV fm
$M_n=8.07131$ MeV	$\kappa_s=2.3$	$c_a=0.145$ MeV	$r_0=1.16$ fm
$a_v=16.000$ MeV	$c_0=5.8$ MeV	$W=35$ MeV	$r_p=0.80$ fm
$a_s=21.13$ MeV	$c_1=\frac{3}{5}\frac{e^2}{r_0}$	$a_{\rm el}=1.433\times10^{-5}$ MeV	$k_f=\left[\frac{9\pi Z}{4A}\right]^{1/3}\frac{1}{r_0}$
$a_{\rm den}=0.99/\sqrt{2}$ fm	$a=0.68$ fm	$h=6.82$ MeV	

ready been included in the effective interaction $\mathbf{V}_{\rm FDSM}$ of the FDSM.

(2) The FDSM shell correction $\langle \mathbf{V}_{\rm FDSM}\rangle$.

The FDSM shell corrections $\langle \mathbf{V}_{\rm FDSM}\rangle$ are obtained by computing the expectation value of the FDSM effective interaction $\mathbf{V}_{\rm FDSM}$. The spherical s.p. energy splittings have already been incorporated in the spherical s.p. shell correction. There is no need to introduce deformed s.p. orbitals since we make no deformed mean-field approximation: Deformation energies are implicitly contained as many-body effects in $\langle \mathbf{V}_{\rm FDSM}\rangle$.

It can be shown that in the symmetry limits (see the Appendix)

$$\begin{aligned}\langle \mathbf{V}_{\rm FDSM}\rangle=&a_\alpha+b_\alpha N_p+c_\alpha N_p^2+d_\alpha N_n+e_\alpha N_n^2+f_\alpha N_pN_n+G_2^\pi\langle\Delta\mathbf{C}^\pi_{\rm Sp6}\rangle_\alpha+G_2^\nu\langle\Delta\mathbf{C}^\nu_{\rm Sp6}\rangle_\alpha\\&+\mathcal{G}_0^\pi\langle\Delta\mathbf{C}^\pi_{\mathcal{SU}2}\rangle_\alpha+\mathcal{G}_0^\nu\langle\Delta\mathbf{C}^\nu_{\mathcal{SU}2}\rangle_\alpha+(G_0^\pi-G_2^\pi)\langle\Delta\mathbf{C}^\pi_{\rm SU2}\rangle_\alpha+(G_0^\nu-G_2^\nu)\langle\Delta\mathbf{C}^\nu_{\rm SU2}\rangle_\alpha\\&+(B_2^\pi-G_2^\pi)\langle\mathbf{C}^\pi_{\rm SU3}\rangle_\alpha+(B_2^\nu-G_2^\nu)\langle\mathbf{C}^\nu_{\rm SU3}\rangle_\alpha+B_2^{\pi\nu}\langle V_Q^{\pi\nu}\rangle_\alpha\quad(\alpha=\mathrm{SU_2},\mathrm{SU_3})\,.\end{aligned}\tag{4.4}$$

In Eq. (4.4) $\langle\mathbf{O}\rangle_\alpha$ stands for the expectation value of the operator $\mathbf{O}$ with the SU_3 wave functions ($\alpha=SU_3$) or SU_2 wave functions ($\alpha=SU_2$), N_p and N_n are the pair numbers of valence protons and neutrons, respectively; $\Delta\mathbf{C}^\sigma_{\rm Sp6}=\mathbf{C}^\sigma_{\rm Sp6}-\Omega_1^\sigma(\Omega_1^\sigma+12)/4$, and $\Delta\mathbf{C}^\sigma_{\rm SU2}=\mathbf{C}^\sigma_{\rm SU2}-\Omega_1^\sigma(\Omega_1^\sigma+2)/4$, with $\sigma=\pi,\nu$. The quantity Ω_1^σ is the pair shell degeneracy of the normal-parity orbitals [$\Omega_1^\sigma=\sum(2j+1)/2$]. The various symbols $\mathbf{C}$ are the Casimir operators of corresponding groups for protons or neutrons. The script $\mathcal{SU}2$ and upper case SU2 are employed to distinguish between the SU_2 symmetry for abnormal- and normal-parity levels, respectively. In the calculation, a variational principle is employed to decide whether the SU_2 or the SU_3 wave function should be used: we calculate each situation and select the one with the lowest energy.

The formulas for computing the expectation values in Eq. (4.4) are listed in Table III. They can be derived straightforwardly following Refs. [6] and [13], except for the SU_3 pairing energy $\langle\mathbf{S}^\dagger(\sigma)\mathbf{S}(\sigma)\rangle_{\rm SU3}$, for which analytical formulas are available for most cases of interest, but which generally can only be computed numerically. The formulas to compute the pairing energies in the SU_3 basis, and a detailed discussion of how the quantum numbers $v_0^\sigma, v_1^\sigma, u_1^\sigma, N_1^\sigma, \lambda_\sigma$, and μ_σ for the ground state of a given nucleus are determined, are given in the Appendix.

It should be noticed that although in this calculation the symmetry-breaking terms are treated as a first-order perturbation, this does not mean that the total mass is computed perturbatively. Taking SU_3 as an example, by perturbative we mean that $\mathbf{S}^\dagger\mathbf{S}$ is treated as a perturbation of the SU_3 ground-state wave function, which is a *nonperturbative condensate* of S and D pairs. The term $\langle\mathbf{S}^\dagger\mathbf{S}\rangle_{\rm SU3}$ induces fluctuations around this correlated ground state. Thus the perturbed state is still a highly

TABLE III. The formulas for computing $\langle \mathbf{V}_{\rm FDSM}\rangle$. The quantum numbers v_0^σ and v_1^σ are seniorities of the SU_2 wave functions for normal- and abnormal-parity levels, respectively; u_1^σ is the heritage quantum number of the Sp_6 group; N_1^σ is the pair number in the normal-parity levels; λ_σ and μ_σ are the conventional SU_3 quantum numbers.

Matrix element	$\alpha=SU_2$	$\alpha=SU_3$
$\langle\Delta\mathbf{C}^\sigma_{\rm Sp6}\rangle_\alpha$	$-\frac{1}{4}(2\Omega_1^\sigma+3)u_1^\sigma$	$-\frac{1}{4}(2\Omega_1^\sigma+3)u_1^\sigma$
$\langle\Delta\mathbf{C}^s_{\mathcal{SU}2}\rangle_\alpha$	$-\frac{1}{4}(2\Omega_0^\sigma+1)v_0^\sigma$	$-\frac{1}{4}(2\Omega_0^\sigma+1)v_0^\sigma$
$\langle\Delta\mathbf{C}^\sigma_{\rm SU2}\rangle_\alpha$	$-\frac{1}{4}(2\Omega_1^\sigma+1)v_1^\sigma$	$\langle\mathbf{S}^\dagger(\sigma)\mathbf{S}(\sigma)\rangle_{\rm SU3}-N_1^\sigma(\Omega_1^\sigma-N_1^\sigma+1)$
$\langle\mathbf{C}^\sigma_{\rm SU3}\rangle_\alpha$	$\frac{5N_1^\sigma(\Omega_1^\sigma-N_1^\sigma)}{\Omega_1^\sigma-1}-\frac{5\Omega_1^\sigma}{4(\Omega_1^\sigma-1)}u_1^\sigma$	$(\lambda_\sigma^2+\mu_\sigma^2+\lambda_\sigma\mu_\sigma+3\lambda_\sigma+3\mu_\sigma)/2$
$\langle\mathbf{V}_Q^{\pi\nu}\rangle_\alpha$	0	$\langle\mathbf{C}^{\pi\nu}_{\rm SU3}-\mathbf{C}^\pi_{\rm SU3}-\mathbf{C}^\nu_{\rm SU3}\rangle_{\rm SU3}$

nonperturbative one with respect to single-particle degrees of freedom. Similarly, for the SU_2 case quadrupole-quadrupole interactions are treated as a perturbation of the SU_2 ground-state wave function, which is again highly nonperturbative (the S pair condensate).

However, in such a first-order-perturbation calculation the phase transition from spherical (described by an SU_2 wave function) to deformed (described by an SU_3 wave function) occurs too suddenly. It is anticipated that the n-p quadrupole-quadrupole interaction $\mathbf{V}_Q^{\pi\nu}$ $[2B_r^{\pi\nu}\mathbf{P}^2(\pi)\cdot\mathbf{P}^2(\nu)]$ is primarily responsible for such a transition. However, as one sees from Table III, the expectation value of $\mathbf{V}_0^{\pi\nu}$ is zero in the SU_2 case, which means that the first-order perturbation is zero. It becomes dominant in the SU_3 case because the magnitude of $\langle \mathbf{C}_{SU3}^{\pi\nu} - \mathbf{C}_{SU3}^{\pi} - \mathbf{C}_{SU3}^{\nu} \rangle_{SU3}$ increases quadratically as the number of valence particles becomes large (subject to Pauli restrictions, $N_1^{\sigma} \leq \Omega_1^{\sigma}/3$, discussed below). In order to provide a smoother SU_2-SU_3 transition, we have included a higher-order correction to $\mathbf{V}_Q^{\pi\nu}$ for the SU_2 case:

$$B_2^{\pi\nu}\langle \mathbf{V}_Q^{\pi\nu}\rangle_{SU2} = \frac{\Delta E_0}{2}\left[1-\left[1+\frac{|\langle \text{g.s.}|V_Q^{\pi\nu}|\text{exc}\rangle|^2}{(\Delta E_0/2)^2}\right]^{1/2}\right], \tag{4.5}$$

where ΔE_0 is the excitation energy of the first vibrational state that can admix with the unperturbed ground state, and $\langle \text{g.s.}|V_Q^{\pi\nu}|\text{exc}\rangle$ is the mixing matrix element of $\mathbf{V}_Q^{\pi\nu}$. The quantities ΔE_0 and $\langle \text{g.s.}|V_Q^{\pi\nu}|\text{exc}\rangle$ can easily be estimated if we assume that the unperturbed ground state is a seniority-zero state and the excited state is a seniority-4 state ($v^{\pi}=v^{\nu}=2$), i.e., $|\text{exc}\rangle = |(2^{\pi}2^{\nu})0\rangle$ for an even-even nucleus. It can be shown that for this case

$$\Delta E_0 = [(G_0^{\pi}-G_2^{\pi})\Omega_1^{\pi}+(G_0^{\nu}-G_2^{\nu})\Omega_1^{\nu}], \tag{4.6a}$$

$$\langle \text{g.s.}|V_Q^{\pi\nu}|\text{exc}\rangle = 2B_2^{\pi\nu}\left[5\frac{N_1^{\pi}(\Omega_1^{\pi}-N_1^{\pi})}{\Omega_1^{\pi}-1}\frac{N_1^{\nu}(\Omega_1^{\nu}-N_1^{\nu})}{\Omega_1^{\nu}-1}\right]^{1/2}. \tag{4.6b}$$

We have assumed that Eq. (4.5) is applicable to an odd system as well. This implies that the low-lying vibrational states are assumed to be seniority excitations of an even-even core.

It should also be noticed that in deriving Eq. (4.4) the pairing and quadrupole-quadrupole couplings between the abnormal- and normal-parity levels are only *formally* neglected. In the strongly deformed region, neglecting the pairing off-diagonal matrix elements may not be a bad approximation. This is because, on the one hand, the energy difference for different SU_3 representations is not small (roughly 1 MeV, which can be estimated from the first β- or γ-band bandhead energy) and, on the other hand, the pairing matrix element itself is already suppressed strongly [as we shall see in Eq. (4.7), the suppression factor is roughly a factor of 3 compared to the SU_2 cases]. However, the quadrupole-quadrupole coupling between abnormal- and normal-parity levels is generally not negligible in the well-deformed region. In the geometrical picture, this corresponds to the energy splitting of the abnormal-parity level due to the deformed mean field. To take such an interaction into account microscopically, one needs to include broken pair (seniority $v\neq 0$) states in the abnormal-parity level. This will complicate matters sufficiently that a large scale numerical calculation will be required.

In this calculation, we have used a simple way to include such an effect that allows us to maintain an analytical form for the mass formula. This is achieved by empirically determining the polynomial coefficients in Eq. (4.4) and allowed different values for the SU_3 and SU_2 cases. It is reasonable to assume that the ground-state energy gain as a function of N_p and N_n due to abnormal-parity level splitting is smooth and can be approximated by a quadratic function. This can be seen by examining the Nilsson model, which we have shown to correspond (quantitatively) to a large particle number approximation of the FDSM [14]. In fact, to a good approximation the abnormal-parity levels split linearly with deformation (which is microscopically proportional to particle number [14(a)]). Therefore, for deformed nuclei the effect of the quadrupole-quadrupole coupling between abnormal- and normal-parity levels is *de facto* included by a renormalization of the coefficients of the polynomial in Eq. (4.4).

The situation is similar for the vibrational case, where the symmetry is SU_2 and the quadrupole coupling is not important. In this case the pairing coupling between abnormal- and normal-parity levels can be computed analytically, and it can be shown explicitly to be a quadratic function of the number of particles. Thus the effect of this coupling is again simply to renormalize the coefficients of the polynomial. By determining these coefficients empirically and allowing then to be different for SU_2 and SU_3, the contributions to the ground-state mass due to the coupling between abnormal- and normal-parity levels are effectively taken into account.

(3) Analytical formula for $82 \leq Z \leq 99$ and $126 \leq N \leq 151$ nuclei.

Since the $\langle \mathbf{S}^{\dagger}(\sigma)\mathbf{S}(\sigma)\rangle_{SU3}$ calculation is rather cumbersome, the FDSM shell correction for the general case can only be computed numerically. However, for $82 \leq Z \leq 99$ and $126 \leq N \leq 151$, which includes virtually all known nuclei in the actinide region, one can derive an analytical expression. The reason is that in this range of Z and N

the particle number in the normal-parity levels [according to Eq. (A3)] is $\leq 2\Omega_1/3$ (i.e., $n_1^\sigma \leq 2\Omega_1^\sigma/3$, $\sigma=\pi$ and ν), and therefore the SU_3 wave functions belong to the symmetric irreducible representation (irrep) $(2N_1^\sigma,0)$. In this case $\langle \mathbf{S}^\dagger(\sigma)\mathbf{S}(\sigma)\rangle_{SU3}$ and thus $\langle \mathbf{V}_{\rm FDSM}\rangle$ have been obtained analytically:

$$\langle \mathbf{S}^\dagger(\sigma)\mathbf{S}(\sigma)\rangle_{SU3}=\frac{2N_1+1}{2N_1-1}N_1^\sigma(\Omega_1^\sigma/3-N_1^\sigma+1) -\frac{2N_1+1}{2N_1-1}\frac{2\Omega_1^\sigma+3}{12}u_1^\sigma , \tag{4.7}$$

where $N_1=N_1^\pi+N_1^\nu$, and

$$\langle \mathbf{V}_{\rm FDSM}\rangle_{SU2}=a_{SU2}+b_{SU2}N_p+c_{SU2}N_p^2+d_{SU2}N_n+e_{SU2}N_n^2+f_{SU2}N_pN_n + \sum_{\sigma=\pi,\nu}\left[(B_2^\sigma-G_2^\sigma)\frac{5N_1^\sigma(\Omega_1^\sigma-N_1^\sigma)}{\Omega_1^\sigma-1}\right]+\Delta_{SU2}^\sigma\delta_{u^\sigma,1}+B_2^{\pi\nu}\langle \mathbf{V}_Q^{\pi\nu}\rangle_{SU2} , \tag{4.8a}$$

$$\langle \mathbf{V}_{\rm FDSM}\rangle_{SU3}=a_{SU3}+b_{SU3}N_p+c_{SU3}N_p^2+d_{SU3}N_n+e_{SU3}N_n^2+f_{SU3}N_pN_n - \sum_{\sigma=\pi,\nu}\left[(G_0^\sigma-G_2^\sigma)\frac{2(N_1-1)}{2N_1-1}\frac{2}{3}\Omega_1^\sigma N_1^\sigma+\frac{2N_1^\sigma(N_1^\sigma-1)}{2N_1-1}\right] + \sum_{\sigma=\pi,\nu}[(B_2^\sigma-G_2^\sigma)N_1^\sigma(2N_1^\sigma+3)+\Delta_{SU3}^\sigma\delta_{u^\sigma,1}]+4B_2^{\pi\nu}N_1^\pi N_1^\nu . \tag{4.8b}$$

In Eq. (4.8), Δ_{SU2}^σ and Δ_{SU3}^σ are constants that are nonzero in the ground state only for odd-A or odd-odd systems (that is, when $u^\sigma=1$, where $u^\sigma=u_1^\sigma+v_1^\sigma+v_0^\sigma$). They correspond physically to the average even-odd mass differences (or pairing gaps) for spherical and deformed nuclei, respectively,

$$\Delta_{SU2}^\sigma=-\mathcal{G}_0^\sigma\tfrac{1}{4}(2\Omega_0^\sigma+1)v_0^\sigma-(G_0^\sigma-G_2^\sigma)\frac{2\Omega_1^\sigma+1}{5}v_1^\sigma - \left[G_2^\sigma\frac{2\Omega_1^\sigma+3}{4}+(B_2^\sigma-G_2^\sigma)\frac{5\Omega_1^\sigma}{4(\Omega_1^\sigma-1)}\right]u_1^\sigma , \tag{4.9a}$$

$$\Delta_{SU3}^\sigma=-\mathcal{G}_0^\sigma\tfrac{1}{4}(2\Omega_0^\sigma+1)v_0^\sigma - \left[G_2^\sigma\frac{2\Omega_1^\sigma+3}{4} +(G_0^\sigma-G_2^\sigma)\frac{2N_1+1}{2N_1-1}\frac{2\Omega_1^\sigma+3}{12}\right]u_1^\sigma . \tag{4.9b}$$

Equations (4.8) and (4.9) can also be applied to the $N_1^\sigma>2\Omega_1^\sigma/3$ (that is, $n_1^\sigma>4\Omega_1^\sigma/3$) case, if N_1^σ in these equations is replaced by the hole number $(\Omega_1^\sigma-N_1^\sigma)$.

(4) Determination of the parameters in version II.

The strengths of monopole and quadrupole pairing, G_0^σ and G_2^σ, respectively, are determined from the first 2^+ state excitation energies of ^{210}Pb and ^{210}Po (0.7997 and 1.1814 MeV, respectively [15]), and the average pairing gap energies for protons and neutrons. The experimental data on pairing gaps can be obtained from the even-odd mass differences. The average pairing gaps for the deformed and spherical nuclei are found to be $\Delta_{SU3}^\pi=0.75$ MeV, $\Delta_{SU3}^\nu=0.63$ MeV, $\Delta_{SU2}^\pi=1.0$ MeV, and $\Delta_{SU2}^\nu=0.86$ MeV, as shown in Fig. 3.

If one assumes that the wave functions of the first 2^+ states of ^{210}Pb and ^{210}Po correspond simply to a D pair of neutrons or protons outside ^{208}Pb, then

$$E_{2^+}(^{210}\mathrm{Po})=-\Omega_1^\pi(G_0^\pi-G_2^\pi)=1.1814\ \mathrm{MeV} , \tag{4.10a}$$

$$E_{2^+}(^{210}\mathrm{Pb})=-\Omega_1^\nu(G_0^\nu-G_\nu^\pi)=0.7997\ \mathrm{MeV} . \tag{4.10b}$$

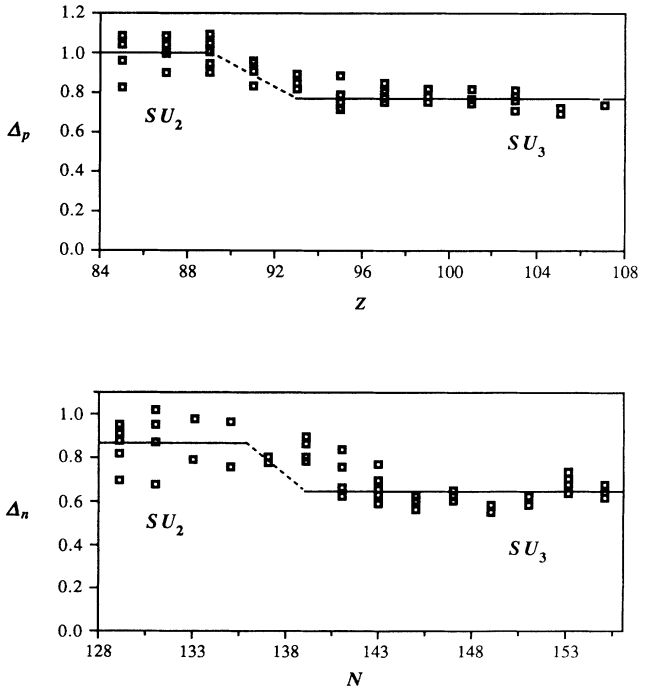

FIG. 3. Pairing gap energies in the actinide region ($Z\geq 82, N\geq 126$). The experimental data (open squares) are obtained from the even-odd mass difference; the solid lines are the FDSM predictions of average pairing gaps in the SU_2 and SU_3 limits using Eq. (4.9). Dashed lines are just drawn as interpolations for transitional nuclei. Experimental masses are taken from Ref. [16].

Also, by assuming that the odd nucleon is in a normal-parity level ($u_1^\sigma = v_1^\sigma = 1$ and $v_0^\sigma = 0$), one can obtain from Eq. (4.9) that

$$\Delta_{SU3}^\pi = -G_2^\pi \frac{2\Omega_1^\pi + 3}{4} - (G_0^\pi - G_2^\pi)\frac{2\Omega_1^\pi + 3}{12} = 0.75 \text{ MeV} , \quad (4.11a)$$

$$\Delta_{SU3}^\nu = -G_2^\nu \frac{2\Omega_1^\nu + 3}{4} - (G_0^\nu - G_2^\nu)\frac{2\Omega_1^\nu + 3}{12} = 0.63 \text{ MeV} , \quad (4.11b)$$

$$\Delta_{SU2}^\pi = -(G_0^\pi - G_2^\pi)\frac{2\Omega_1^\pi + 1}{4} - G_2^\pi \frac{2\Omega_1^\nu + 3}{4} - (B_2^\pi - G_2^\pi)\frac{5\Omega_1^\pi}{4(\Omega_1^\pi - 1)} = 1.0 \text{ MeV} , \quad (4.12a)$$

$$\Delta_{SU2}^\nu = -(G_0^\nu - G_2^\nu)\frac{2\Omega_1^\nu + 1}{4} - G_2^\nu \frac{2\Omega_1^\nu + 3}{4} - (B_2^\nu - G_2^\nu)\frac{5\Omega_1^\nu}{4(\Omega_1^\nu - 1)} = 0.86 \text{ MeV} . \quad (4.12b)$$

We will discuss below the implications if the odd nucleon is not in a normal-parity level.

Knowing these values, and that for $82 \le Z \le 126$ and $126 \le N \le 184$ the degeneracies are $\Omega_1^\pi = 15$ and $\Omega_1^\nu = 21$, from (4.10) and (4.11) one can immediately obtain values for $(G_0^\sigma - G_2^\sigma)$ and G_2^σ. In principle one can also determine B_2^σ from Eq. (4.12). However, we found that these parameters are small and poorly determined ($B_2^\pi \approx 0.03 \pm 0.1$ and $B_2^\nu \approx 0.026 \pm 0.04$). Hence, for simplicity we have set them to zero. This is consistent with the common belief that the quadrupole-quadrupole interaction among like particles is small compared with the *n-p* quadrupole-quadrupole interaction. To summarize, the parameters obtained here are

$$(G_0^\pi - G_2^\pi) = -0.078 \text{ MeV} , \quad G_2^\pi = -0.064 \text{ MeV}, \; B_2^\pi \approx 0 ; \quad (4.13a)$$

$$(G_0^\nu - G_2^\nu) = -0.038 \text{ MeV} , \quad G_2^\nu = -0.044 \text{ MeV}, \; B_2^\nu \approx 0 . \quad (4.13b)$$

From Eqs. (4.11) and (4.12) one sees that not only monopole pairing, but also quadrupole pairing, will contribute to the energy gap (even-odd mass differences). Nevertheless, it has been shown [6(b)] that to consider both monopole and quadrupole pairing is equivalent to considering an effective monopole pairing with a strength $(G_0^\sigma - G_2^\sigma)$ plus a term $G_2^\sigma \times C_{Sp6}^\sigma$, where C_{Sp6}^σ is the expectation value of the Sp_6 Casimir operator. The latter depends only on heritage number u_1^σ, and therefore is merely a constant, although it does contribute to the energy gap. In Eqs. (4.11) and (4.12), the terms $-G_2^\sigma[(2\Omega_1^\sigma + 3)/4]$ originate from Sp_6 Casimir operator and the terms $-(G_0^\sigma - G_2^\sigma)[(2\Omega_1^\sigma + 1)/4]$ and $-(G_0^\sigma - G_2^\sigma)[(2\Omega_1^\sigma + 3)/12]$ are the SU_2 and SU_3 pairing gaps, respectively. Using the values of Eq. (4.13), the effective pairing gaps are 0.605 MeV for protons and 0.409 MeV for neutrons. These are the two pairing gaps used in the calculation of pairing shell corrections.

It should be noted that an ambiguity exists in the derivation of Eqs. (4.11) and (4.12), because we have assumed that the odd particle is in a normal-parity level. This is probably a reasonable assumption at the beginning or the end of the shell (mainly the SU_2 case), since the abnormal orbitals are near midshell for this mass region (see Fig. 1). However, for deformed nuclei (the SU_3 case), it is possible that the odd particle resides in the abnormal orbital. In that case, $u_1^\sigma = v_1^\sigma = 0$ and $v_0^\sigma = 1$, and the gap formulas will be changed to

$$\Delta_{SU3}^\pi = -\mathcal{G}_{0\frac{1}{4}}^\pi (2\Omega_0^\pi + 1) = 0.75 \text{ MeV} , \quad (4.14a)$$

$$\Delta_{SU3}^\nu = -\mathcal{G}_{0\frac{1}{4}}^\nu (2\Omega_0^\nu + 1) = 0.63 \text{ MeV} . \quad (4.14b)$$

Of course, if the ground-state parity is measured for a given nucleus, one can identify whether the odd particle is in a normal- or abnormal-parity orbital and then use the appropriate formula. However, data indicate that the pairing gap is relatively independent of which orbital the odd particles occupies. For convenience in the present calculation we have assumed that the odd particle is always in the normal-parity orbital. Nevertheless, one can take advantage of Eq. (4.14) to determine the pairing strength in the abnormal-parity level. The abnormal levels for heavy and superheavy nuclei ($82 \le Z \le 126$ and $126 \le N \le 184$) are i_{132} for protons and $J_{15/2}$ for neutrons; therefore, $\Omega_0^\pi = 7$ and $\Omega_0^\nu = 8$ and one obtains

$$\mathcal{G}_0^\pi = -0.20 \text{ MeV}, \quad \mathcal{G}_0^\nu = -0.15 \text{ MeV} . \quad (4.15)$$

Thus, we have reduced the number of adjustable parameters in the FDSM-Strutinsky mass formula from 16 in version I to 13 in version II. These 13 parameters are determined by fitting 332 known actinide-region masses. They are found to be the following (in units of MeV).

For Woods-Saxon spherical s.p. energies: $B_2^{\pi\nu} = -0.0912$,

$$a_\alpha = -13.75, \; b_\alpha = -4.572, \; c_\alpha = 0.4293 , \quad d_\alpha = -4.889, \; e_\alpha = 0.3306, \; f_\alpha = -0.2915 \quad (\alpha = \text{SU2}) ; \quad (4.16a)$$

$$a_\alpha = -5.570, \; b_\alpha = -5.790, \; c_\alpha = 0.3713 , \quad d_\alpha = -6.806, \; e_\alpha = 0.3587, \; f_\alpha = -0.1095 \quad (\alpha = \text{SU3}) .$$

For equal spacing spherical s.p. energies: $B_2^{\pi\nu} = -0.0899$,

$$a_\alpha=-13.75,\ b_\alpha=-4.313,\ c_\alpha=0.4182,$$
$$d_\alpha=-5.007,\ e_\alpha=0.3248,\ f_\alpha=-0.2976$$
$$(\alpha=\text{SU2});\quad (4.16b)$$

$$a_\alpha=-6.506,\ b_\alpha=-5.300,\ c_\alpha=0.3319,$$
$$d_\alpha=-6.826,\ e_\alpha=0.3530,\ f_\alpha=-0.1105$$
$$(\alpha=\text{SU3}).$$

For experimental spherical s.p. energies: $B_2^{\pi\nu}=-0.0909$,

$$a_\alpha=-13.75,\ b_\alpha=-4.882,\ c_\alpha=0.4300,$$
$$d_\alpha=-4.983,\ e_\alpha=0.3316,\ f_\alpha=-0.3005$$
$$(\alpha=\text{SU2});\quad (4.16c)$$

$$a_\alpha=-4.158,\ b_\alpha=-6.198,\ c_\alpha=0.3808,$$
$$d_\alpha=-7.154,\ e_\alpha=0.3568,\ f_\alpha=-0.1045$$
$$(\alpha=\text{SU3}).$$

V. RESULTS

With Eq. (4.4) and the previously determined parameters, we are in a position to compute masses for heavy and superheavy nuclei ($82\le Z\le 126$ and $126\le N\le 184$). Discrepancies between the computed and the experimentally known masses are displayed in Fig. 4. The total shell correction $M_{\rm sh}$ as well as neutron and proton separation energies are shown in Figs. 5, 6, and 7. For comparison, the Möller-Nix calculations (referred to as MN) are also shown. It is clear that for this mass region the FDSM mass formula is an improvement over the Möller-Nix results. (The Möller-Nix mass formula also applies to other mass regions. A global comparison of the two theories awaits the extension of the present FDSM calculation to these other regions.) This improvement is particularly obvious at the light and heavy ends. At the light end (vibrational region), we see that not only does the FDSM give a smaller rms discrepancy in the shell corrections, but the unphysical irregularities in the separation energies S_p and S_n of the Möller-Nix calculations (see Figs. 6 and 7) are not present. At the heavy end, one sees that MN systematically predict less bound systems, while the FDSM results agree well with data (see Fig. 5). This latter improvement is particularly important in the effort to extrapolate to the unknown heavy regions.

The above-mentioned improvements of the FDSM mass formula over the mass formulas such as MN are due basically to two physical reasons. (i) The FDSM inherently contains SU_2 and SU_3 dynamical symmetries. These symmetries can describe well both the vibrational (SU_2) and rotational (SU_3) limits. The Möller-Nix mass formula is based on the deformed mean-field approximation, which is expected to be a reasonable approximation for nuclei with stable deformations. This could be the reason why irregularities occur in the vibrational regions for such calculations. (ii) The FDSM directly treats the pairing and quadrupole interactions as two-body interactions, without introducing a deformed mean-field approximation. Hence many-body correlations are better taken into account. Also, the approach does not suffer appreciably from the number nonconservation caused by the BCS approximation, nor the angular momentum fluctuations inherent in a deformed mean-field approximation. Conversely, in the mean-field approach, one anticipates that some important many-body correlations may be lost. As we shall see below, there is a suggestion that the systematic deficit of binding energy for heavy elements that characterizes the MN calculations may be related specifically to the failure to include explicitly or effectively the monopole-monopole interactions.

Before pursuing this point further, let us discuss the dynamical Pauli effect. This effect can be seen clearly in Fig. 8. This figure assumes (incorrectly, for illustration) that the SU_3 ground-state wave function is always in the symmetric representation: $(\lambda,\mu)=(n_1,0)$. The discrepancy between experiment and theory is essentially zero until the valence proton pair number $N_p=8$ and neutron pair number $N_n=13$ are reached. After that, the discrepancy begins to increase linearly. Note that according to Eq. (A11), $N_p=8.5$ (i.e., $Z=99$) and $N_n=12.5$

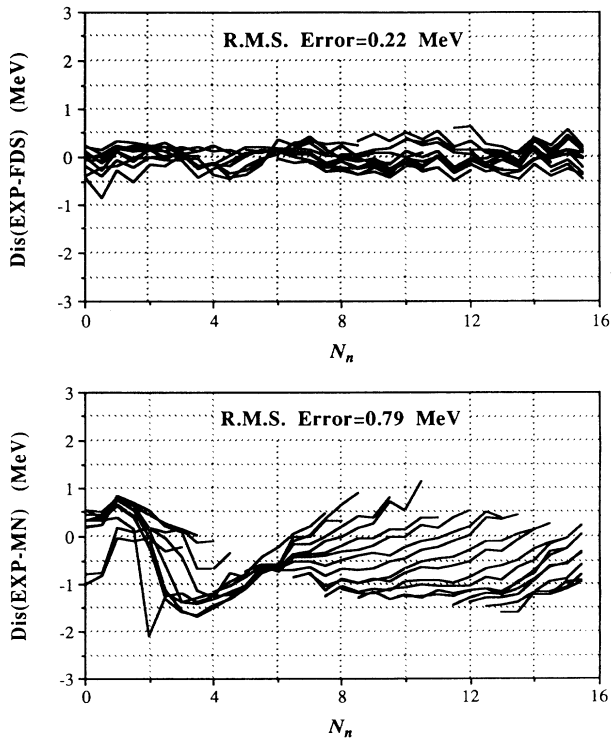

FIG. 4. The discrepancy between experiment and theory in heavy nuclear mass calculations ($Z\ge 82, N\ge 126$). The top figure is the discrepancy for the FDSM calculation using Woods-Saxon single-particle energies. For comparison, the Möller-Nix calculation [5] is shown at the bottom. Data are taken from Ref. [16]. Different curves correspond to different proton numbers.

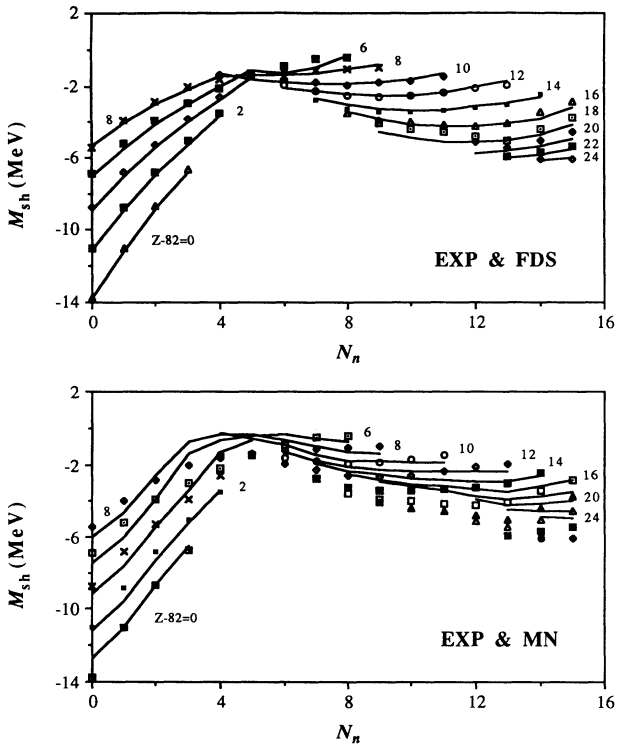

FIG. 5. The shell corrections for heavy nuclear masses ($Z \geq 82, N \geq 126$). The top figure is the FDSM calculation using Woods-Saxon single-particle energies; for comparison, the Möller-Nix calculation [5] is shown in the bottom figure. The curves are theoretical predictions and the symbols are data [16]. For clarity, only even-even nuclei are presented.

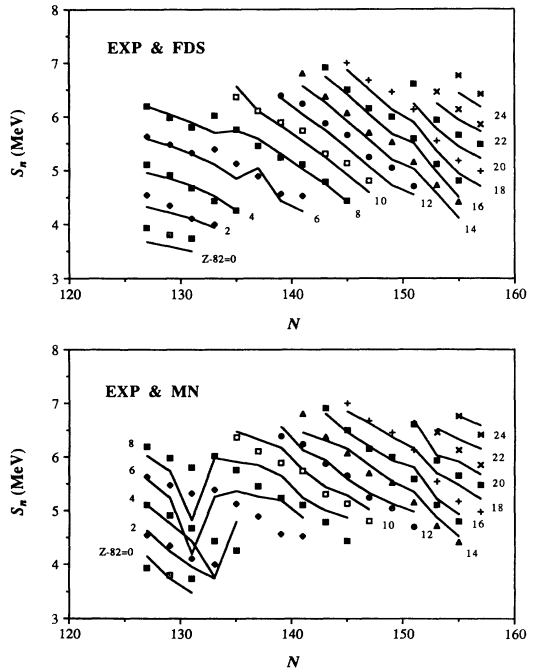

FIG. 6. Neutron separation energies for heavy elements ($Z \geq 82, N \geq 126$). The top figure is the result of the FDSM calculation using Woods-Saxon single-particle energies. For comparison, we show Möller-Nix calculations [5] in the bottom figure. The curves are theoretical calculations and the symbols are data [16].

($N=151$) are exactly the numbers of valence proton and neutron pairs in the normal-parity levels N_1^π and N_1^ν corresponding to the threshold for departure from ground-state symmetric representations: $\Omega_1^\pi/3$ and $\Omega_1^\nu/3$, respectively. This result seems to provide rather convincing evidence that (i) when $N_1^\sigma \leq \Omega_1^\sigma/3$ ($\sigma=\pi,\nu$), the $SU_3(n_1,0)$ representation is a good description for the ground state of a deformed nucleus, at least in the actinide region; and (ii) when $N_1^\sigma > \Omega_1^\sigma/3$ the nuclear ground state is no longer described by the $(n_1,0)$ representation. Instead, higher representations will be more favored. This is consistent with the FDSM predictions, since $(n_1,0)$ in this case is Pauli forbidden. Indeed, when the dynamical Pauli effect is taken into account by requiring (correctly) that the ground state be the lowest Pauli-allowed representation [see Eq. (A14)], all the large discrepancies of Fig. 8 disappear (cf. Fig. 4).

The dynamical Pauli effect appears also in the neutron separation energies, which we display in Figs. 6. Here one sees that the calculated neutron separation energies have a kink at $N=151$ ($N_1^\nu=\Omega_1^\nu/3$). There is a suggestion that the data exhibit a similar kink. From the FDSM point of view, this kink is also due to the dynamical Pauli effect: When the neutron number goes beyond $N=151$ there is a phase transition from an SU_3 symmetric representation to an asymmetric representation, for which the ground-state energy is higher. This additional drop in separation energy adds to the continuous decrease as neutron number increases and causes a kink. A similar situation for proton separation energy can also be seen in the FDSM calculation, but the effect is small and it is difficult to detect it clearly in the data (Fig. 7).

It is quite interesting that a similar kink appears in the MN calculations of the neutron separation energy at pre-

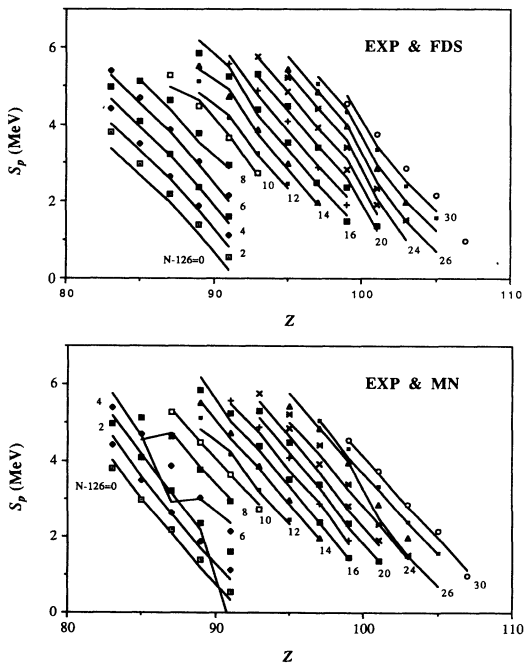

FIG. 7. Proton separation energies for heavy elements ($Z \geq 82, N \geq 126$). Details as in Fig. 6.

cisely the same location. Since the deformed mean field knows nothing directly about group representations, this requires some explanation. The occurrence of such a kink in the MN approach is presumably due to the large $Z=98$ and $N=152$ energy gaps in the deformed s.p. spectrum. It is not surprising that these two shell gaps occur at the same particle number as the dynamical Pauli effect. When the symmetric SU_3 representation is allowed only up to a certain particle number, say $N=152$, adding one more nucleon will cause the nucleus to acquire a more than an average amount of energy, because the many-body system will be forced by the Pauli principle to move to an asymmetric representation, which is less bound. In the mean-field language, this is equivalent to the introduction of a s.p. energy gap at $N=152$. This means that the deformed mean fields in common use (e.g., Nilsson or deformed Woods-Saxon models) include at least part of the dynamical Pauli effect through empirical adjustment of s.p. parameters to reproduce observed nuclear properties. (See Fig. 8.)

Thus the empirical appearance of deformed shell gaps at $Z=98$ or $N=152$ acquires a *fundamental* interpretation in the FDSM: these gaps are consequences of an $Sp_6 \supset SU_3$ symmetry of the many-body collective wave function. Their location is correctly predicted by the theory in terms of the number of particles occupying normal-parity orbitals, independent of the detailed s.p. structure. This is in contrast to the usual deformed mean-field approach, where the appearance of gaps (and the corresponding Strutinsky shell corrections) is a consequence of the detailed properties of the s.p. energies for many orbitals. Since these are ultimately dependent on phenomenology, such an approach offers no fundamental explanation of these shell gaps.

An important feature in the mass shell correction for heavy nuclei (Fig. 5) is that on the heavy end M_{sh} tends to bend upward. For $Z>98$ and $N>152$, the upward behavior of M_{sh} is partially related to the dynamical Pauli

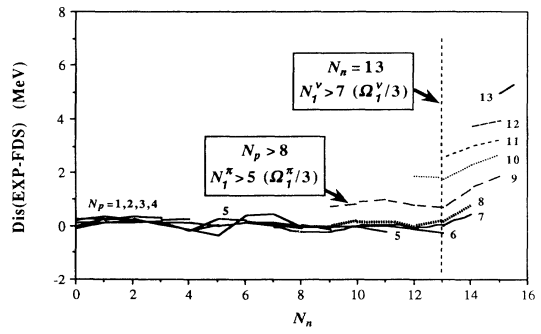

FIG. 8. Dynamical Pauli effect in heavy nuclear masses ($Z\geq 82, N\geq 126$). For clarity in the figure only even-even nuclei are presented. The theoretical mass used in this figure is the calculation with the same parameters as in Fig. 4, except that one assumes (incorrectly) that the ground-state SU_3 wave function is the symmetric $(n_1,0)$ representation $(n_1=n_1^\pi+n_1^\nu)$. When the dynamical Pauli effect is taken into account by using the correct representation (see text), the large discrepancies for $N_p>8$ and $N_n>13$ vanish, as we have seen in Fig. 4.

effect, as was explained above: When the number of valence particles is increased between $2\Omega_1^\sigma/3$ and Ω_1^σ, the expectation value of the SU_3 Casimir operator will decrease, thus causing the shell correction to become less negative. However, the upward trend one observes in Fig. 5 actually begins earlier than $Z=98$ and $N=152$ (which correspond to $N_p=8$ and $N_n=13$, respectively). Hence the reason for the increase in this region cannot be the dynamical Pauli effect alone. An additional source is found to be the quadratic number-dependent terms ($c_\alpha N_p^2$ and $e_\alpha N_n^2$) in the polynomial of Eq. (4.4), which originate from the monopole-monopole interactions of the two-body Hamiltonian.

To see this more clearly, let us separate out the monopole-monopole interactions from the polynomial of Eq. (4.4) which is the expectation value of the $\mathbf{V}_0(\mathbf{N}_0^\pi,\mathbf{N}_1^\pi,\mathbf{N}_0^\nu,\mathbf{N}_1^\nu)$ term in Eq. (A3). Using $\mathbf{V}_{sym}$ to denote the symmetry-dependent terms, Eq. (4.4) can be expressed as

$$\langle \mathbf{V}_{FDSM}\rangle=\langle \mathbf{V}_0\rangle+\langle \mathbf{V}_{sym}\rangle \ . \tag{5.1}$$

On the other hand, as shown in the Appendix Eq. (A2), $\mathbf{V}_{FDSM}$ can be expressed as a sum of monopole-monopole interactions $\mathbf{V}_{mono}$ and the FDSM pairing plus quadrupole interactions $\mathbf{V}_{pq}$ (including quadrupole pairing), thus

$$\langle \mathbf{V}_{FDSM}\rangle=\langle \mathbf{V}_{mono}\rangle+\langle \mathbf{V}_{pq}\rangle \ . \tag{5.1'}$$

Using Eqs (A4), it is easy to obtain the following relations:

$$\begin{aligned}\langle \mathbf{V}_{mono}\rangle&=\langle \mathbf{V}_0\rangle-\langle \mathbf{V}_{sym}^0\rangle \ ,\\ \langle \mathbf{V}_{pq}\rangle&=\langle \mathbf{V}_{sym}\rangle+\langle \mathbf{V}_{sym}^0\rangle \ ,\end{aligned} \tag{5.2}$$

where

$$\begin{aligned}\langle \mathbf{V}_{sym}^0\rangle=\sum_{\sigma=\pi,\nu}[&G_2^\sigma N_1^\sigma(\Omega_1^\sigma-N_1^\sigma+6)\\&+\mathcal{G}_0^\sigma N_0^\sigma(\Omega_0^\sigma-N_0^\sigma+1)\\&+(G_0^\sigma-G_2^\sigma)N_1^\sigma(\Omega_1^\sigma-N_1^\sigma+1)] \ .\end{aligned} \tag{5.3}$$

Thus, knowing $\langle \mathbf{V}_0\rangle$ and $\langle \mathbf{V}_{sym}\rangle$ one can obtain $\langle \mathbf{V}_{mono}\rangle$ and $\langle \mathbf{V}_{pq}\rangle$, and the total mass shell correction (4.1b) can be expressed as

$$M_{sh}=M_{sh}^{s.p.}+V_{sh}^{pair}+\langle \mathbf{V}_{mono}\rangle+\langle \mathbf{V}_{pq}\rangle \ . \tag{5.4}$$

A typical example of the behavior of each term in Eq. (5.4) and its contribution to the mass shell correction is shown in Fig. 9. The dynamical Pauli effect shows up here as the $\mathbf{V}_{pq}$ curve begins its upward climb at $N\sim 152$. However, the $\mathbf{V}_{mono}$ curve bends upward earlier (at $N\sim 146$) and much stronger. This strength is due to the repulsive quadratic number-dependent terms in the monopole-monopole interactions. It is this repulsiveness, together with the dynamical Pauli effect, that dictates the upward trend of the shell corrections at the heavy end. The lack of such repulsive terms presumably gives rise to a smaller upward curvature in the MN mass shell correction curves as seen in Fig. 5. This may be the reason why the MN predictions at the heavy end tend to be less

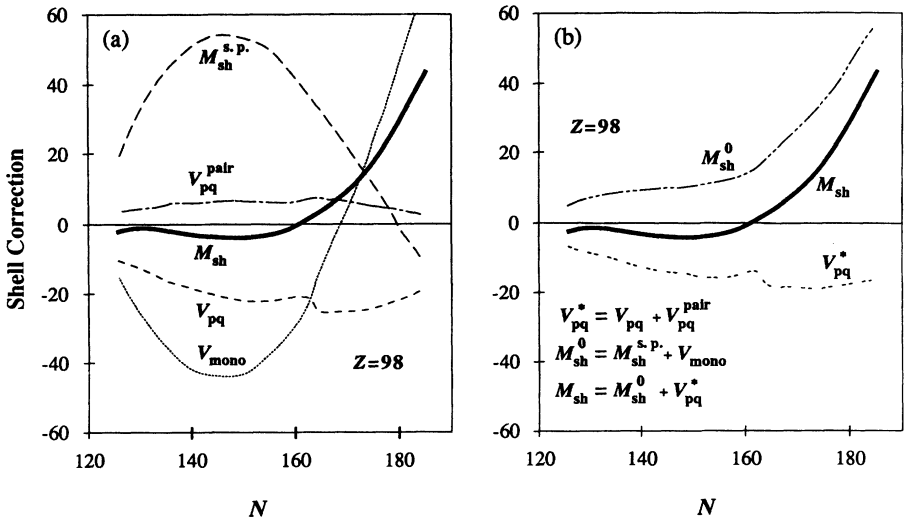

FIG. 9. Components of the mass shell corrections for $Z=98$ nuclei [see Eq. (5.4)]. In diagram (a) the behavior as a function of neutron number N for each component in the mass shell correction is given. The kinks shown on the V_{pq} and V_{mono} curves at $N=162$ originate from the $SU_3(N\leq 162)\rightarrow SU_2(N>162)$ phase transition. In diagram (b) the behavior of $(M_{sh}^{s.p.}+V_{mono})$ and $(V_{pq}+V_{sh}^{pair})$ are given. The solid line shown in each diagram is the total mass shell correction M_{sh}. For clarity, only the results for even-even nuclei are presented.

bound (or overbound, if parameters are readjusted to fine-tune the agreement in the intermediate region).

From Fig. 9 one may notice that the FDSM also predicts a large positive mass shell correction for very neutron-rich nuclei (in this $Z=98$ example, when $N=184$, $M_{sh}=39$ MeV). A similar situation occurs for the very proton-rich side (e.g., when $Z=126$ and $N=126$, $M_{sh}=22$ MeV). At first glance this seems unusual since no known nucleus or previous mass calculation has ever shown such large positive mass shell corrections. However, it should be noted that, on one hand, the large positive shell corrections predicted by the FDSM occur only in the region far from the β-stability line (very neutron rich or proton rich), and there are no known nuclei there. Near the β-stability region, where data exist, the FDSM predicts no contradiction to the data because the repulsive *n-n* and *p-p* monopole-monopole interactions are largely canceled by an attractive *n-p* monopole-monopole interaction (the $f_\alpha N_p N_n$ term). On the other hand, since previous mass calculations have not taken the monopole-monopole interaction into account, which is the source of the large repulsiveness, it is not surprising that these approaches predict no large positive shell correction in any case. The large difference in the region far from the β-stability line may have significant consequences in nuclear astrophysics. Thus it would be very interesting to check whether this large positive mass shell correction is realistic. A radioactive beam facility might provide answers to this important question.

We wish to emphasize that the appearance of quadratic number-dependent monopole-monopole terms in the expression for nuclear masses is a natural consequence of a general two-body interaction. In fact, it is well known that in the multipole expansion of the residual nucleon-nucleon interaction the monopole-monopole interaction is the leading term. However, since this interaction depends only on particle numbers, for a given nucleus it will only contribute a constant energy and essentially will have no effect on the low-lying nuclear structure, where the particle number distribution change is not anticipated to be dramatic. This may explain why the monopole-monopole interaction terms have previously not received much attention and have often been neglected. Obviously, such terms must affect the ground-state energy and should be present in a realistic mass formula. It should be mentioned that Pittel *et al.* have emphasized the importance of monopole-monopole interactions in several publications [17]. They suggested that it is the *n-p* monopole-monopole interactions that cause single-particle energies to change from the beginning of a shell to the end of the shell. The present analysis suggests that in addition to the *n-p* attractive monopole-monopole interaction there exist *n-n* and *p-p* monopole-monopole interactions as well, and that these have an important repulsive contribution to the masses of very heavy elements.

We now see that the FDSM mass formula is simple, analytic for most nuclei in the actinide region, and can be computed rapidly. Therefore it is convenient for systematic studies. As an example, we have computed all the ground-state nuclear masses for $82\leq Z\leq 126$ and $126\leq N\leq 184$ with three different sets of s.p. energies (see Fig. 1). Our aim in this example is to study the dependence of the energy minimum of superheavy elements on the variation of the s.p. energies. As we have shown in Fig. 10, a deep minimum is located at $Z=114$ and $N=164$ for the Woods-Saxon case. The corresponding shell correction is $M_{sh}=-12.6$ MeV, which is comparable to the large shell correction of ^{208}Pb (-13.75 MeV).

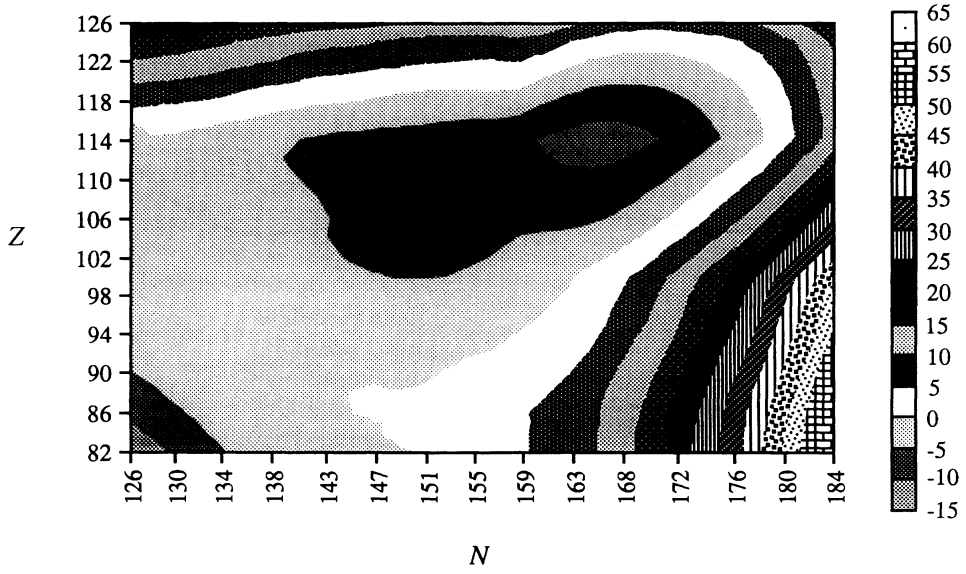

FIG. 10. Contour plot of the mass shell correction for heavy and superheavy elements using Woods-Saxon single-particle energies. The predicted minimum for superheavy elements is $^{278}_{114}X_{164}$.

On the other hand, for the equal spacing s.p. case the minimum is at $Z=116$, $N=170$, and $M_{\rm sh}=-14.7$ MeV. When we use the experimental s.p. energies, a rather flat minimum is at $Z=122-124$ and $N=176-180$, and $M_{\rm sh}=-18.0\sim-18.1$ MeV. For each set of s.p. energies the superheavy elements are predicted to be spherical (SU_2 symmetry). In all three cases the rms error is 0.22–0.23 MeV.

It is understandable why the overall fit to the known masses is not sensitive to the differences of these three s.p. level schemes. The first three s.p. levels are nearly identical in all three schemes for protons and neutrons (see Fig. 1), and nucleons of known nuclei mainly occupy these levels. The dramatic differences in the s.p. levels for these schemes occur mainly in the second half of the shell, as can be seen in Fig. 1. Unfortunately, the ground states of existing nuclei do not have large occupancy in these levels. One anticipates that the masses of superheavy elements will be more sensitive to the s.p. structure of the second half of the shell, and according to our calculations, that is indeed the case. In fact, we see in Fig. 11 that different s.p. schemes do give rise to different results in the superheavy region. Among the three s.p. schemes, the experimental one is the most compressed and has the largest level density at the end of the shell (see Fig. 1). This makes the experimental s.p. scheme (among the three considered) to have the largest negative s.p. shell correction at the end of the shell (see Fig. 11),

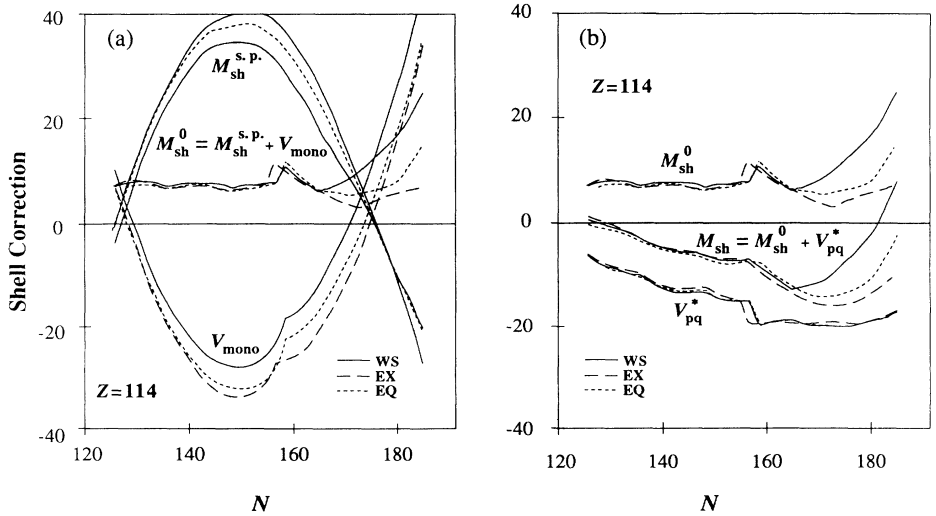

FIG. 11. The $Z=114$ mass shell corrections for three different s.p. level schemes. WS stands for Woods-Saxon potential, EQ for equal spacing, and EX for experimental s.p. spectra. In diagram (a), the spherical s.p. shell correction $M_{\rm sh}^{\rm s.p.}$ and the monopole-monopole interaction $V_{\rm mono}$ and their sum $M_{\rm sh}^0$ are shown. The kink around $N=156$ is caused by the $SU_3\rightarrow SU_2$ phase transition. In diagram (b), $M_{\rm sh}^0$, $V_{\rm pq}^*$ ($V_{\rm pq}^*=V_{\rm pq}+V_{\rm sh}^{\rm pair}$) and their sum are shown. For clarity, only results for even-even nuclei are presented.

and explains why this scheme prefers to push the superheavy minimum toward the heavy end of the shell and makes it more bound. Since at the moment there are no data to ascertain which s.p. scheme is preferred, we feel that no definite prediction about the superheavy elements can be made. Nevertheless, the fact that the three different s.p. schemes all predict a deep minimum for the mass shell correction in the superheavy region (although the locations are different) seems to give an encouraging signal about the existence of the superheavy island. Of course, a large negative mass shell correction does not automatically ensure the existence of superheavy elements. In particular, the stability of such superheavy elements with respect to fission and α decay needs to be further explored before more definitive statements can be made.

The situation for the monopole-monopole interactions is similar: At present, no quantitative statement can be made about the interaction strengths since different s.p. schemes lead to different monopole-monopole interactions (the difference can be as large as 20 MeV at the heavy end of the shell) and yet give essentially the same quality fit for known masses. Nevertheless, the importance of the monopole-monopole interactions in the microscopic mass calculations can already be recognized. As can be seen from Figs. 9 and 11, the spherical s.p. shell corrections $M_{\rm sh}^{\rm s.p.}$ and the monopole-monopole interactions $\mathbf{V}_{\rm mono}$ are the two largest components of the mass shell correction. Both can contribute as much as 50 MeV, which is much larger than the other terms in the mass shell correction (5.4). However, $M_{\rm sh}^{\rm s.p.}$ is always convex in shape while $\mathbf{V}_{\rm mono}$ is always concave, and they tend to cancel each other strongly. It is this cancellation of $M_{\rm sh}^{\rm s.p.}$ and $\mathbf{V}_{\rm mono}$ which makes their sum comparable to the pairing plus quadrupole interactions contributions, which then add to give the final mass shell correction. Without the monopole-monopole interactions, it is difficult to imagine how (within the framework of a spherical shell model) the mass shell correction can be correctly computed. The next step, which is now underway, is to apply this approach to the rare earths, since the s.p. level scheme there is less ambiguous and data are more complete. We anticipate that one will learn more about the monopole-monopole interactions there, even though they will be weaker because N_p and N_n are smaller.

The success of the version II FDSM mass formula discussed in this paper clearly suggests that a correct treatment of the spherical s.p. shell correction is crucial to a microscopic understanding of the FDSM mass formula, and of how it can be extended to general mass calculations. Our method, as presented in this paper, is now ready to be applied to other regions of the nuclear chart. This work is now in progress. Finally, in a forthcoming article, we shall discuss the astrophysical r process using version II of the mass formula [17]. Preliminary results suggest that there are substantial improvements in some crucial aspects of r-process calculations when the FDSM mass formula is substituted for more traditional mass formulas.

ACKNOWLEDGMENTS

We would like to express thanks for the useful discussions we had with James Truran, Friedel Thielemann, and Art Champagne about the astrophysical implications of nuclear masses. Useful discussions on various aspects of nuclear masses with Nissan Zeldes, Bruce Barrett, Rong-Ping Wang, and Zhen-Ping Li are also appreciated. This work is partially supported by the United States National Science Foundation, the Department of Energy, and the Chinese National Natural Science Foundation.

APPENDIX: THE FDSM HAMILTONIAN AND WAVE FUNCTIONS

1. The FDSM Hamiltonian

The original FDSM Hamiltonian for the heritage $u=0$ case (heritage u is the number of particles that do not form S and D pairs, $u=u_1^\pi+u_1^\nu+v_0^\pi+v_0^\nu$) is as follows [6]:

$$\mathbf{H}_{\rm FDSM}=\sum_{\sigma=\pi,\nu}(n_0^\sigma e_0^\sigma+n_1^\sigma e_1^\sigma)+\mathbf{V}_{\rm FDSM}\ , \tag{A1a}$$

$$\mathbf{V}_{\rm FDSM}=\mathbf{V}^\pi+\mathbf{V}^\nu+\mathbf{V}^{\pi\nu}\ , \tag{A1b}$$

$$\mathbf{V}^\sigma=\mathcal{B}_0^\sigma N_0^\sigma N_0^\sigma+B_0^\sigma N_1^\sigma N_1^\sigma+b_0^\sigma N_0^\sigma N_1^\sigma+\mathcal{G}_0^\sigma\mathcal{S}^\dagger(\sigma)\mathcal{S}(\sigma)+G_0^\sigma\mathbf{S}^\dagger(\sigma)\mathbf{S}(\sigma)+G_2^\sigma\mathbf{D}^\dagger(\sigma)\cdot\mathbf{D}(\sigma)+\sum_{r=1,2}B_r^\sigma\mathbf{P}^r(\sigma)\cdot\mathbf{P}^r(\sigma)$$
$$+g_0^\sigma[\mathbf{S}^\dagger(\sigma)\mathcal{S}(\sigma)+\mathcal{S}^\dagger(\sigma)\mathbf{S}(\sigma)]\quad(\sigma=\pi,\nu)\ , \tag{A1c}$$

$$\mathbf{V}^{\pi\nu}=\sum_{r=1,2}2B_r^{\pi\nu}\mathbf{P}^r(\pi)\cdot\mathbf{P}^r(\nu)+B_0^{\pi\nu}N_1^\pi N_1^\nu+\mathcal{B}_0^{\pi\nu}N_0^\pi N_0^\nu+b_0^{\pi\nu}(N_0^\pi N_1^\nu+N_1^\pi N_0^\nu)\ , \tag{A1d}$$

where e_0^σ and e_1^σ are the average single-particle energies for the abnormal- and normal-parity levels; n_0^σ and n_1^σ are the corresponding particle numbers ($N_i^\sigma=n_i^\sigma/2$); $\mathcal{S}^\dagger(\sigma)[\mathcal{S}(\sigma)]$, $\mathbf{S}^\dagger(\sigma)[\mathbf{S}(\sigma)]$, and $\mathbf{D}^\dagger(\sigma)$ $[\mathbf{D}(\sigma)]$ are the creation [annihilation] operators for S pairs in the abnormal-parity levels, and S and D pairs in normal-parity levels, respectively. A detailed definition of these terms can be found in Ref. [6]. For odd nuclei we have assumed that the same Hamiltonian should be used, but with different wave functions; namely, the heritage must be changed from $u=0$ to $u=u^\pi=1$ ($u=u^\nu=1$) for odd Z (odd N), or $u^\pi=u^\nu=1$ ($u=2$) for odd-odd nuclei.

The FDSM effective interaction $\mathbf{V}_{\rm FDSM}$ can be grouped into three terms: monopole-monopole interactions $\mathbf{V}_{\rm mono}$, pairing plus quadrupole-quadrupole interactions $\mathbf{V}_{\rm pq}$, and an angular momentum coupling term $\mathbf{V}_J$:

$$\mathbf{V}_{\rm FDSM}=\mathbf{V}_{\rm mono}+\mathbf{V}_{\rm pq}+\mathbf{V}_J\ , \tag{A2a}$$

$$\mathbf{V}_{\rm mono}=\sum_{\sigma=\pi,\nu}\mathcal{B}_0^\sigma N_0^\sigma N_0^\sigma+B_0^\sigma N_1^\sigma N_1^\sigma+b_0^\sigma N_0^\sigma N_1^\sigma+B_0^{\pi\nu}N_1^\pi N_1^\nu+\mathcal{B}_0^{\pi\nu}N_0^\pi N_0^\nu+b_0^{\pi\nu}(N_0^\pi N_1^\nu+N_1^\pi N_0^\nu)\ , \tag{A2b}$$

$$\mathbf{V}_{\rm pq}=\sum_{\sigma=\pi,\nu}[\mathcal{G}_0^\sigma\mathcal{S}^\dagger(\sigma)\mathcal{S}(\sigma)+G_0^\sigma\mathbf{S}^\dagger(\sigma)\mathbf{S}(\sigma)+G_2^\sigma\mathbf{D}^\dagger(\sigma)\cdot\mathbf{D}(\sigma)+B_2^\sigma\mathbf{P}^2(\sigma)\cdot\mathbf{P}^2(\sigma)]$$
$$+\sum_{\sigma=\pi,\nu}g_0^\sigma[\mathbf{S}^\dagger(\sigma)\mathcal{S}(\sigma)+\mathcal{S}^\dagger(\sigma)\mathbf{S}(\sigma)]+2B_1^{\pi\nu}\mathbf{P}^1(\pi)\cdot\mathbf{P}^1(\nu)\ , \tag{A2c}$$

$$\mathbf{V}_J=\tfrac{3}{8}\left[\sum_{\sigma=\pi,\nu}B_1^\sigma\mathbf{J}_\sigma^2+B_1^{\pi\nu}(\mathbf{J}^2-\mathbf{J}_\pi^2-\mathbf{J}_\nu^2)\right]\ . \tag{A2d}$$

The angular momentum coupling term originates from $\mathbf{P}^1(\sigma)\cdot\mathbf{P}^1(\sigma)$ terms in (A1), since $\mathbf{P}^1(\sigma)=\frac{3}{8}\mathbf{J}_\sigma$ (see Ref. [6]).

Equation (A2) can be rewritten in terms of Casimir operators of the Sp_6, SU_2, and SU_3 groups [using Table VI and Eq. (4.7a) in Ref. [6(b)]]:

$$\mathbf{V}_{\rm FDSM}=V_0(\mathbf{N}_0^\pi,\mathbf{N}_1^\pi,\mathbf{N}_0^\nu,\mathbf{N}_1^\nu)+\sum_{\sigma=\pi,\nu}[G_2^\sigma\Delta\mathbf{C}_{\rm Sp6}^\sigma+\mathcal{G}_0^\sigma\Delta\mathbf{C}_{\mathcal{SU}2}^\sigma+(G_0^\sigma-G_2^\sigma)\Delta\mathbf{C}_{\rm SU2}^\sigma+(B_2^\sigma-G_2^\sigma)\mathbf{C}_{\rm SU3}^\sigma+\tfrac{3}{8}(B_1^\sigma-B_2^\sigma)\mathbf{J}_\sigma^2]$$
$$+B_2^{\pi\nu}(\mathbf{C}_{\rm SU3}^{\pi\nu}-\mathbf{C}_{\rm SU3}^\pi-\mathbf{C}_{\rm SU3}^\nu)+\tfrac{3}{8}(B_1^{\pi\nu}-B_2^{\pi\nu})(\mathbf{J}^2-\mathbf{J}_\pi^2-\mathbf{J}_\nu^2)+\sum_{\sigma=\pi,\nu}g_0^\sigma[\mathbf{S}^\dagger(\sigma)\mathcal{S}(\sigma)+\mathcal{S}^\dagger(\sigma)\mathbf{S}(\sigma)]\ . \tag{A3}$$

In Eq. (A3), V_0 is a quadratic function of the number operators $\mathbf{N}_0^\pi$, $\mathbf{N}_1^\pi$, $\mathbf{N}_0^\nu$, and $\mathbf{N}_1^\nu$. It originates from the monopole-monopole interactions and the transformation from the pairing operators ($\mathbf{S}^\dagger\mathbf{S}$, $\mathcal{S}^\dagger\mathcal{S}$, and $\mathbf{D}^\dagger\mathbf{D}$) to the $SU_2(\mathcal{SU}_2)$ and Sp_6 Casimir operators. The quantities $\mathbf{J}_\pi$, $\mathbf{J}_\nu$, and $\mathbf{J}$ are the angular momenta for protons and neutrons, and the total spin of the ground state, respectively. To derive Eq. (A3) from Eq. (A2) the following relations have been used:

$$\mathbf{S}^\dagger(\sigma)\mathbf{S}(\sigma)=\Delta\mathbf{C}_{\rm SU2}^\sigma+N_1^\sigma(\Omega_1^\sigma-N_1^\sigma+1)\ , \tag{A4a}$$

$$\mathcal{S}^\dagger(\sigma)\mathcal{S}(\sigma)=\Delta\mathbf{C}_{\mathcal{SU}2}^\sigma+N_0^\sigma(\Omega_0^\sigma-N_0^\sigma+1)\ , \tag{A4b}$$

$$\mathbf{S}^\dagger(\sigma)\mathbf{S}(\sigma)+\mathbf{D}^\dagger(\sigma)\mathbf{D}(\sigma)+\mathbf{P}^1(\sigma)\cdot\mathbf{P}_1(\sigma)+\mathbf{P}^2(\sigma)\cdot\mathbf{P}^2(\sigma)$$
$$=\Delta\mathbf{C}_{\rm Sp6}^\sigma+N_1^\sigma(\Omega_1^\sigma-N_1^\sigma+6)\ , \tag{A4c}$$

$$\mathbf{P}^2(\sigma)\cdot\mathbf{P}^2(\sigma)=\mathbf{C}_{\rm SU3}^\sigma-\tfrac{3}{8}\mathbf{J}_\sigma^2\ , \tag{A4d}$$

$$\mathbf{P}^2\cdot\mathbf{P}^2=\mathbf{C}_{\rm SU3}^{\pi\nu}-\tfrac{3}{8}\mathbf{J}^2\quad[\mathbf{P}^2=\mathbf{P}^2(\pi)+\mathbf{P}^2(\nu)]\ . \tag{A4e}$$

To obtain $\langle\mathbf{V}_{\rm FDSM}\rangle$ [Eq. (4.4)] from Eq. (A3), we have neglected the spin-dependent terms. These terms may be important for the spectra, in particular for high-spin states, but are negligible for ground-state masses at the present accuracy. The pairing interaction between normal- and abnormal-parity states, $g_0^\sigma[\mathbf{S}^\dagger(\sigma)\mathcal{S}(\sigma)+\mathcal{S}^\dagger(\sigma)\mathbf{S}(\sigma)]$, is also neglected since its diagonal matrix element vanishes. The quadratic polynomial of N^σ in $\langle\mathbf{V}_{\rm FDSM}\rangle$ is obtained from $\langle\mathbf{V}_0\rangle$ by transforming N_0^σ and N_1^σ into N^σ.

2. The determination of N_1^σ

The relation between N_0^σ, N_1^σ, and N^σ can be obtained from the FDSM: $N_1^\sigma=a+bN$, where a and b are specific combinations of the parameters of the FDSM effective interaction [6]. Empirically, they are found to be ~0.75 and ~0.5, respectively, for the known heavy nuclei [10(a)]:

$$N_1^\sigma=0.75+0.5N^\sigma\ ,\quad N_0^\sigma=-0.75+0.5N^\sigma$$
$$(N^\sigma=N_0^\sigma+N_1^\sigma)\ . \tag{A5a}$$

The average number distribution among normal- and abnormal-parity levels determined by this semiempirical formula is in good agreement with the Nilsson scheme at the appropriate deformation, and has been applied successfully to other calculations [8]. Having Eq. (A5a), for a given nucleus the occupation numbers N_0^σ and N_1^σ are completely determined. However, some caution should be exercised here. First of all, this N_1^σ value should be interpreted as an average value that need not have integer or half-integer values. Second, when $N^\sigma\le1$, or $N^\sigma>2\Omega_0^\sigma+1.5$, Eq. (A5a) violates number conservation and should not be used. In this case, N_1^σ is determined as follows:

$$N_1^\sigma=\begin{cases}N^\sigma & \text{for } N^\sigma\le1\ ,\\ N^\sigma-\Omega_0^\sigma & \text{for } N^\sigma>2\Omega_0^\sigma+1.5\ ,\end{cases} \tag{A5b}$$

which is simply the requirement of number conservation. Third, although Eq. (A5) describes the average behavior quite well, there are local fluctuations about the average. There are various reasons for such fluctuations: deviations from the symmetry limit not accounted for in the present calculations, symmetry changes from SU_2 to SU_3 or from the symmetric SU_3 representation to nonsymmetric representations, etc. A more precise treatment would account for such local modifications of Eq. (A5).

3. The SU_2 and SU_3 wave functions

The ground-state wave functions are assumed to have either $SU_3^{\pi+\nu}\times\mathcal{SU}_2^\pi\times\mathcal{SU}_2^\nu$ symmetry (denoted as SU_3 wave functions for short) or $SU_2^\pi\times SU_2^\nu\times\mathcal{SU}_2^\pi\times\mathcal{SU}_2^\nu$ symmetry (denoted as SU_2), depending on whether the nucleus is deformed or spherical:

$$SU_3:\quad|v_0^\pi N_0^\pi u_1^\pi N_1^\pi(\lambda_\pi\mu_\pi),v_0^\nu N_0^\nu u_1^\nu N_1^\nu(\lambda_\nu\mu_\nu);(\lambda\mu)\tau J\rangle\ , \tag{A6a}$$

$$\mathrm{SU}_2: \quad |v_0^{\pi}N_0^{\pi}u_1^{\pi}N_1^{\pi}(v_1^{\pi}),v_0^{\nu}N_0^{\nu}u_1^{\nu}N_1^{\nu}(v_1^{\nu});\tau J\rangle \ . \tag{A6b}$$

As noted above, the choice between these possibilities is dictated by minimizing the energy of the ground state at fixed particle number.

In Eqs. (A6a) and (A6b), J is the ground-state spin and τ is the additional quantum number necessary to specify the state. The indices 0 and 1 denote the abnormal- or normal-parity levels, respectively.

The $\mathrm{SU}_3^{\pi+\nu}$ wave function in Eq. (A6a) can also be labeled by the U_3 quantum numbers

$$|[u_1^{\pi}][\omega^{\pi}],[u_1^{\nu}][\omega^{\nu}];[\omega]\rangle \ ,$$

where

$$\begin{aligned} &2N_1=\omega_1+\omega_2+\omega_3 \ , \quad [\omega]\equiv[\omega_1,\omega_2,\omega_3] \ , \\ &\lambda=\omega_1-\omega_2, \quad \mu=\omega_2-\omega_3 \ ; \end{aligned} \tag{A7a}$$

$$\begin{aligned} &2N_1^{\sigma}=\omega_1^{\sigma}+\omega_2^{\sigma}+\omega_3^{\sigma} \ , \quad [\omega^{\sigma}]\equiv[\omega_1^{\sigma},\omega_2^{\sigma},\omega_3^{\sigma}] \ , \\ &\lambda^{\sigma}=\omega_1^{\sigma}-\omega_2^{\sigma}, \quad \mu^{\sigma}=\omega_2^{\sigma}-\omega_3^{\sigma} \ . \end{aligned} \tag{A7b}$$

The ground-state heritage and seniority numbers are simply determined by whether the neutron and proton numbers are odd or even

$$u^{\sigma}=u_1^{\sigma}+v_0^{\sigma}=\begin{cases} 0 & n^{\sigma}=\text{even}, \ v_1^{\sigma}=u_1^{\sigma} \ , \\ 1 & n^{\sigma}=\text{odd}, \ v_1^{\sigma}=u_1^{\sigma} \ . \end{cases} \tag{A8}$$

The SU_3 quantum numbers $(\lambda_{\sigma},\mu_{\sigma})$ and (λ,μ) are determined by n_1^{σ}, the particle number in the normal-parity levels. For an attractive quadrupole-quadrupole interaction the symmetric representation $(\lambda_{\sigma},\mu_{\sigma})=(n_1^{\sigma},0)$ and $(\lambda,\mu)=(n_1^{\pi}+n_1^{\nu},0)$ for particles, or $(0,\bar{n}_1^{\sigma})$ and $(0,\bar{n}_1^{\pi}+\bar{n}_1^{\nu})$ for $\bar{n}_1^{\sigma}$ holes (where $\bar{n}_1^{\sigma}=2\Omega_1^{\sigma}-n_1^{\sigma}$), is usually the SU_3 ground state. However, when the particle number $\Omega_1^{\sigma}\geq n_1^{\sigma}>2\Omega_1^{\sigma}/3$ or $\Omega_1^{\sigma}>\bar{n}_1^{\sigma}>2\Omega_1^{\sigma}/3$ (i.e., $2\Omega_1^{\sigma}/3<n_1^{\sigma}<4\Omega_1^{\sigma}/3$) the symmetric representations $(\lambda_{\sigma},\mu_{\sigma})=(n_1^{\sigma},0)$ or $(0,\bar{n}_1^{\sigma})$ are Pauli forbidden. This is the *dynamical Pauli effect,* which requires the allowed SU_3 representations for the ground state to be

$$(\lambda_{\sigma},\mu_{\sigma})=\begin{cases} (n_1^{\sigma},0), & n_1^{\sigma}\leq 2\Omega_1^{\sigma}/3 \ , \\ (4\Omega_1^{\sigma}/3-n_1^{\sigma},n_1^{\sigma}-2\Omega_1^{\sigma}/3), & 2\Omega_1^{\sigma}/3<n_1^{\sigma}\leq 4\Omega_1^{\sigma}/3 \ , \\ (0,2\Omega_1^{\sigma}-n_1^{\sigma}), & n_1^{\sigma}>4\Omega_1^{\sigma}/3 \ , \end{cases} \tag{A9a}$$

and

$$(\lambda,\mu)=(\lambda_{\pi}+\lambda_{\nu},\mu_{\pi}+\mu_{\nu}) \ . \tag{A9b}$$

Thus, for a given nucleus the quantum numbers of the ground state are determined from (A5), (A8), and (A9), and the FDSM shell correction can be computed in accordance with the formulas given in Table III.

4. The formula for $\langle \mathbf{S}^{\dagger}(\sigma)\mathbf{S}(\sigma)\rangle_{\mathrm{SU3}}$

Using $|[u_1^{\sigma}][\omega^{\sigma}],[u_1^{\tau}][\omega^{\tau}];[\omega]\rangle$ to specify an SU_3 wave function for $2N_1$ particles, and $|[u_1^{\sigma}][\tilde{\omega}^{\sigma}],[u_1^{\tau}][\omega^{\sigma}];[\omega']\rangle$ for $2N_1-2$ particles, where the symbols $[\omega^{\sigma}]$ and $[\omega]$ are the U_3 quantum numbers for the $2N_1^{\sigma}$ and $2N_1$ system defined in Eq. (A7), and $[\tilde{\omega}^{\sigma}]$ and $[\omega']$ are the U_3 quantum numbers for the $2N_1^{\sigma}-2$ and $2N_1-2$ systems, the matrix element can be computed in the following way:

$$\langle \mathbf{S}^{\dagger}(\sigma)\mathbf{S}(\sigma)\rangle_{\mathrm{SU3}}=\sum_{[\tilde{\omega}^{\sigma}],[\omega']} |\langle [u_1^{\sigma}][\omega^{\sigma}],[u_1^{\tau}][\omega^{\tau}];[\omega]\|\mathbf{S}^{\dagger}(\sigma)\|[u_1^{\sigma}][\tilde{\omega}^{\sigma}],[u_1^{\tau}][\omega^{\tau}];[\omega']\rangle|^2 \ , \tag{A10a}$$

where

$$\begin{aligned} &\langle [u_1^{\sigma}][\omega^{\sigma}],[u_1^{\tau}][\omega^{\tau}];[\omega]\|\mathbf{S}^{\dagger}(\sigma)\|[u_1^{\sigma}][\tilde{\omega}^{\sigma}],[u_1^{\tau}][\omega^{\tau}];[\omega']\rangle \\ &\qquad =U([2],[\tilde{\omega}^{\sigma}],[\omega],[\omega^{\tau}];[\omega^{\sigma}],[\omega'])\langle [\omega'],[2]\|[\omega]\rangle\langle [u_1^{\sigma}][\omega^{\sigma}]\|\|A\|\|[u_1^{\sigma}][\tilde{\omega}^{\sigma}]\rangle \end{aligned} \tag{A10b}$$

and

$$\begin{aligned} \langle [u_1^{\sigma}][\omega^{\sigma}]\|\|A\|\|[u_1^{\sigma}][\tilde{\omega}^{\sigma}]\rangle &=\frac{\sqrt{3}}{2}[\Lambda_{[n^{\sigma}][\omega^{\sigma}]}-\Lambda_{[\bar{n}^{\sigma}][\tilde{\omega}^{\sigma}]}]^{1/2}\langle [n^{\sigma}]\|Z\|[\bar{n}^{\sigma}]\rangle \\ &\quad \times U([u_1^{\sigma}],[\bar{n}^{\sigma}],[\omega^{\sigma}],[2];[\tilde{\omega}^{\sigma}],[n^{\sigma}]) \ . \end{aligned} \tag{A10c}$$

In Eq. (A10c) $[\bar{n}^{\sigma}]$ and $[n^{\sigma}]$ are the U_3 quantum numbers for the $2N_1^{\sigma}-u_1^{\sigma}-2$ and $2N_1^{\sigma}-u_1^{\sigma}$ systems, respectively.

The U coefficients in Eq. (A10c) are the U_3, or equivalently SU_3, Racah coefficients; $\langle [\omega'],[2]\|[\omega]\rangle$ is an SU_3 Clebsch-Gordan coefficient; the factor $[\Lambda_{[n^{\sigma}][\omega^{\sigma}]}-\Lambda_{[\bar{n}^{\sigma}][\tilde{\omega}^{\sigma}]}]$ has been computed previously by Hecht [see Eq. (34) and Table III in Ref. [13(a)]]; the reduced matrix element $\langle [n^{\sigma}]\|Z\|[\bar{n}^{\sigma}]\rangle$ can be computed using Eq. (2.25) of Ref. [13(b)]. Explicit expressions for the pairing matrix elements can be found in Ref. [13(c)] for most of the important physical cases.

[1] J. J. Cowan, F.-K. Thielemann, and J. W. Truran, Phys. Rep. (to be published).

[2] W. A. Fowler and C. C. Meisl, in *Cosmogenical Processes,* edited by W. D. Arnett, C. J. Hansen, J. W. Truran, and S. Tsuruta (VNU, Singapore, 1986), p. 83; F. K. Thielemann and J. W. Truran in *Nucleosynthesis and its Implications in Nuclear and Particle Physics,* edited by J. Audouze (Reidel, Dordrecht, 1986), p. 373.

[3] See, for example, the special issue on nuclear masses in At. Data Nucl. Data Tables **39** (1988).

[4] V. M. Strutinsky, Nucl. Phys. **A95**, 420 (1967); **A122**, 83 (1968).

[5] P. Möller and J. R. Nix, At. Data Nucl. Data Tables **39**, 213 (1988).

[6] (a) C.-L. Wu, D. H. Feng, X. -G. Chen, J.-Q. Chen, and M. W. Guidry, Phys. Lett. B **168**, 313 (1986); (b) Phys. Rev. C **36**, 1157 (1987); (c) C.-L. Wu, in *Proceedings of the Workshop On Microscopic Models in Nuclear Structure Physics,* Oak Ridge National Laboratory, 1988, edited by M. W. Guidry, J. H. Hamilton, D. H. Feng, N. R. Johnson, and J. B. McGrory (World Scientific, Singapore, 1989), p. 21.

[7] C.-L. Wu, X.-L. Han, Z.-P. Li, M. W. Guidry, and D. H. Feng, Phys. Lett. B **194**, 447 (1987).

[8] D. H. Feng, in *Proceedings of the Workshop on Microscopic Models in Nuclear Structure Physics* [7], p. 74.

[9] C.-L. Wu, *Proceedings of The Symposium in Honor of Akito Arima,* Nuclear Physics in the 1990's, Santa Fe, New Mexico, 1990 [Nucl. Phys. **A522**, 31c (1991)].

[10] (a) D. H. Feng, C.-L. Wu, M. W. Guidry, and Z.-P. Li, Phys. Lett. B **205**, 156 (1988); (b) W. M. Zhang, D. H. Feng, C.-L. Wu, and M. W. Guidry, J. Phys. G **15**, L115 (1989); (c) C.-L. Wu, M. W. Guidry, D. H. Feng, and J.-Q. Chen, Fizika **22**, 123 (1990).

[11] H. v. Groote, E. R. Hilf, and K. Takashashi, At. Data Nucl. Data Tables **17**, 418 (1976).

[12] W. D. Myers, At. Data Nucl. Data Tables **17**, 411 (1976).

[13] (a) K. T. Hecht, Nucl. Phys. **A484**, 61 (1988); (b) D. J. Rowe, J. Math. Phys. **25**, 2662 (1984); (c) J.-Q. Chen, X.-G. Chen, D. H. Feng, J. N. Ginocchio, and M. W. Guidry, Phys. Rev. C **40**, 2844 (1989).

[14] (a) H. Wu, D. H. Feng, C.-L. Wu, and M. W. Guidry, Phys. Rev. C **37**, 1739 (1988); (b) C.-L. Wu *et al.* (to be published).

[15] M. Sakai, At. Data Nucl. Data Tables **31**, 399 (1984).

[16] A. H. Wapstra and G. Audi, Nucl. Phys. **A432**, 1 (1985).

[17] S. Pittel and B. Barrett, Ann. Phys. (N.Y.) **176**, 114 (1987); S. Pittel, C. D. Duval, and B. R. Barrett, *ibid.* **144**, 168 (1982); J. Engel, S. Pittel, and P. Vogel, Phys. Rev. Lett. **67**, 426 (1991); J. Engel, P. Vogel, Xiangdong Ji, and S. Pittel, Phys. Lett. B **225**, 5 (1989).

[18] R.-P. Wang, F. K. Thielemann, D. H. Feng, and C.-L. Wu (unpublished).

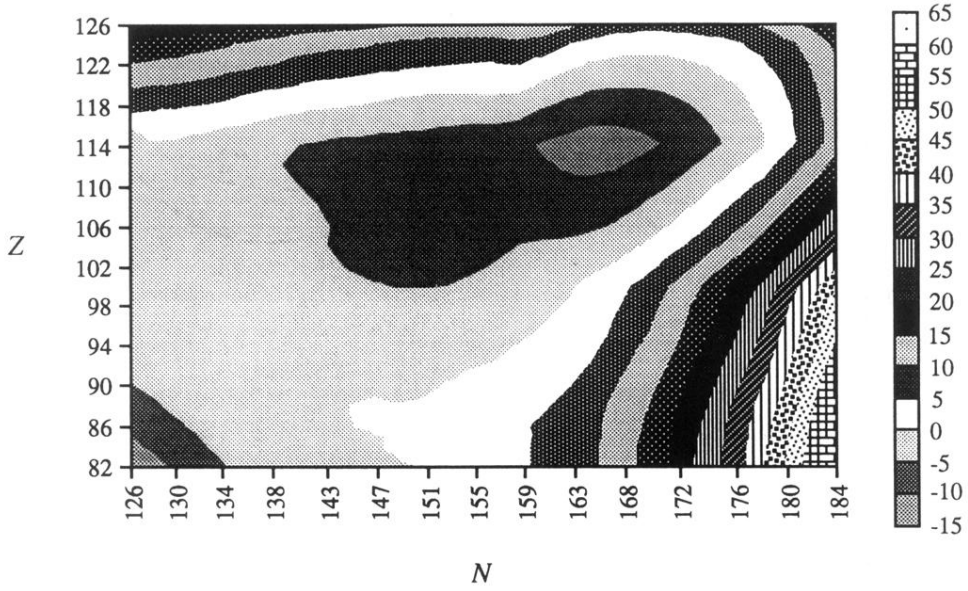

FIG. 10. Contour plot of the mass shell correction for heavy and superheavy elements using Woods-Saxon single-particle energies. The predicted minimum for superheavy elements is ${}^{278}_{114}X_{164}$.